CENTER FOR MECHANICS OF COMPOSITES

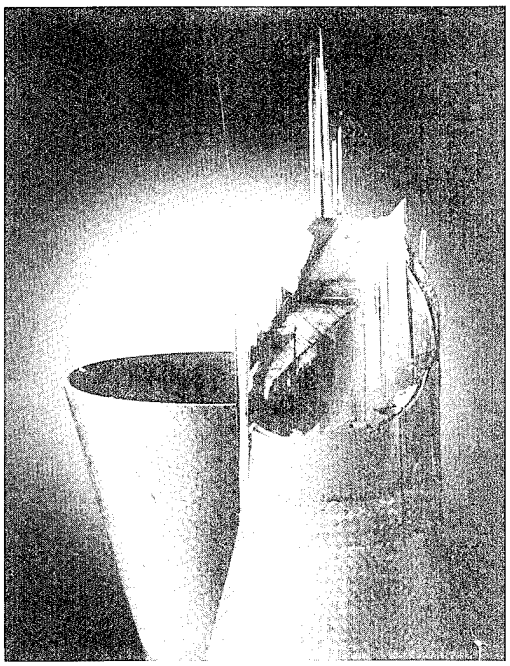

MICROMECHANICS MODELING AND ANALYSIS OF HAVERSIAN COMPACT BONE TISSUE AS A FIBER REINFORCED COMPOSITE MATERIAL

FINAL TECHNICAL REPORT
AFOSR Grant No. F49620-92-J-0208
CMC REPORT NO. 95-01

Submitted to:
Dr. Walter F. Jones, Program Manager
AFOSR/NA

TEXAS ENGINEERING EXPERIMENT STATION

THE TEXAS A&M UNIVERSITY SYSTEM

May 1995

REPORT DOCUMENTATION PAGE

Form Approved
OMB No. 0704-0188

1. AGENCY USE ONLY *(Leave blank)*	2. REPORT DATE	3. REPORT TYPE AND DATES COVERED
	11 May 95	Annual Technical, 1 Apr 92 to 31 Dec 94

4. TITLE AND SUBTITLE
Micromechanics Modeling and Analysis of Haversian Compact Bone Tissue as a Fiber Reinforced Composite Material

5. FUNDING NUMBERS
F49620-92-J-0208

6. AUTHOR(S)
Harry A. Hogan

7. PERFORMING ORGANIZATION NAME(S) AND ADDRESS(ES)
Texas A&M Research Foundation
Texas Engineering Experiment Station
Center for Mechanics of Composites
Department of Mechanical Engineering
College Station, Texas 77843

8. PERFORMING ORGANIZATION REPORT NUMBER

9. SPONSORING/MONITORING AGENCY NAME(S) AND ADDRESS(ES)
United States Air Force
AFOSR/NA
Bolling AFB, DC 20332

10. SPONSORING/MONITORING AGENCY REPORT NUMBER

11. SUPPLEMENTARY NOTES

12a. DISTRIBUTION/AVAILABILITY STATEMENT
Unlimited

12b. DISTRIBUTION CODE

13. ABSTRACT *(Maximum 200 words)*

Haversian compact bone tissue is being studied theoretically and experimentally to characterize its behavior as a fiber reinforced composite material with the aim of biomimicking its salient features. Analytical and finite element based composite micromechanics techniques have been developed and evaluated for theoretical modeling of structure/property relationships. Two-dimensional finite element models of material representative volume elements have been used to predict variations in macroscopic mechanical properties with porosity, constituent properties, and fiber/matrix interface conditions. Mori-Tanaki effective medium methods have also been examined. Haversian compact bone possesses a distinct 'interphase' material surrounding each osteon called the cement line. The role and properties of the cement line are of particular interest for possible biomimicking. Mechanical testing of bone specimens is accompanying the theoretical work to provide data for verification and model improvement. Anisotropic elastic moduli have been measured using through-transmission ultrasound. Longitudinal tensile strength and elastic modulus have been determined from quasi-static tensile testing. In addition, dynamic mechanical testing has been initiated to measure viscoelastic properties. (storage & loss moduli, loss factor). Testing results are also being correlated with quantitative microstructural measures. The parameters of interest include bulk density (wet & dry), mineralization (ash), porosity, osteon area fraction, and total cement line perimeter (per unit area). Additional dynamic testing is continuing to more definitively determine the influence of the cement line on properties.

14. SUBJECT TERMS	15. NUMBER OF PAGES
biomimetics, composite micromechanics, compact bone tissue	35
	16. PRICE CODE

17. SECURITY CLASSIFICATION OF REPORT	18. SECURITY CLASSIFICATION OF THIS PAGE	19. SECURITY CLASSIFICATION OF ABSTRACT	20. LIMITATION OF ABSTRACT
unclassified	unclassified	unclassified	

GENERAL INSTRUCTIONS FOR COMPLETING SF 298

The Report Documentation Page (RDP) is used in announcing and cataloging reports. It is important that this information be consistent with the rest of the report, particularly the cover and title page. Instructions for filling in each block of the form follow. It is important to ***stay within the lines*** to meet ***optical scanning requirements***.

Block 1. Agency Use Only *(Leave blank)*.

Block 2. Report Date. Full publication date including day, month, and year, if available (e.g. 1 Jan 88). Must cite at least the year.

Block 3. Type of Report and Dates Covered. State whether report is interim, final, etc. If applicable, enter inclusive report dates (e.g. 10 Jun 87 - 30 Jun 88).

Block 4. Title and Subtitle. A title is taken from the part of the report that provides the most meaningful and complete information. When a report is prepared in more than one volume, repeat the primary title, add volume number, and include subtitle for the specific volume. On classified documents enter the title classification in parentheses.

Block 5. Funding Numbers. To include contract and grant numbers; may include program element number(s), project number(s), task number(s), and work unit number(s). Use the following labels:

C	- Contract	**PR**	- Project
G	- Grant	**TA**	- Task
PE	- Program Element	**WU**	- Work Unit Accession No.

Block 6. Author(s). Name(s) of person(s) responsible for writing the report, performing the research, or credited with the content of the report. If editor or compiler, this should follow the name(s).

Block 7. Performing Organization Name(s) and Address(es). Self-explanatory.

Block 8. Performing Organization Report Number. Enter the unique alphanumeric report number(s) assigned by the organization performing the report.

Block 9. Sponsoring/Monitoring Agency Name(s) and Address(es). Self-explanatory.

Block 10. Sponsoring/Monitoring Agency Report Number. *(If known)*

Block 11. Supplementary Notes. Enter information not included elsewhere such as: Prepared in cooperation with...; Trans. of...; To be published in.... When a report is revised, include a statement whether the new report supersedes or supplements the older report.

Block 12a. Distribution/Availability Statement. Denotes public availability or limitations. Cite any availability to the public. Enter additional limitations or special markings in all capitals (e.g. NOFORN, REL, ITAR).

- **DOD** - See DoDD 5230.24, "Distribution Statements on Technical Documents."
- **DOE** - See authorities.
- **NASA** - See Handbook NHB 2200.2.
- **NTIS** - Leave blank.

Block 12b. Distribution Code.

- **DOD** - Leave blank.
- **DOE** - Enter DOE distribution categories from the Standard Distribution for Unclassified Scientific and Technical Reports.
- **NASA** - Leave blank.
- **NTIS** - Leave blank.

Block 13. Abstract. Include a brief *(Maximum 200 words)* factual summary of the most significant information contained in the report.

Block 14. Subject Terms. Keywords or phrases identifying major subjects in the report.

Block 15. Number of Pages. Enter the total number of pages.

Block 16. Price Code. Enter appropriate price code *(NTIS only)*.

Blocks 17. - 19. Security Classifications. Self-explanatory. Enter U.S. Security Classification in accordance with U.S. Security Regulations (i.e., UNCLASSIFIED). If form contains classified information, stamp classification on the top and bottom of the page.

Block 20. Limitation of Abstract. This block must be completed to assign a limitation to the abstract. Enter either UL (unlimited) or SAR (same as report). An entry in this block is necessary if the abstract is to be limited. If blank, the abstract is assumed to be unlimited.

MICROMECHANICS MODELING AND ANALYSIS OF HAVERSIAN COMPACT BONE TISSUE AS A FIBER REINFORCED COMPOSITE MATERIAL

FINAL TECHNICAL REPORT

AFOSR Grant No. F49620-92-J-0208

Project Period: April 1, 1992 to December 31, 1994

Submitted to:

Dr. Walter F. Jones, Program Manager

Prepared by:

Harry A. Hogan, Associate Professor

Department of Mechanical Engineering
Texas A&M University

Center for Mechanics of Composites
Texas Engineering Experiment Station

College Station, Texas 77843-3123

May 11, 1995

TABLE OF CONTENTS

INTRODUCTION

This research is part of the recent AFOSR initiative in *Biomimetics*, which has the broad overall goal of seeking to elucidate and understand the salient characteristics of naturally occurring biological composite materials, with an aim toward mimicking these features in devising improved man-made composite materials. The biological composite of interest in this effort is bone tissue, or more specifically Haversian compact bone tissue. A major underlying task in this project is to develop a more deterministic understanding of the relationships between microstructural details and macroscopic mechanical behavior. The unique fiber/matrix interphase material, which is distinctive of this type of bone tissue, is of particular interest because of the recognized significance of interfaces in developing new higher performance composites. The approach combines composite micromechanics modeling techniques to analytically model structure/property relationships with companion experimental testing of tissue samples to evaluate and validate the modeling.

The specific objectives of the project as stated in the original proposal were:

- To develop a two-dimensional micromechanics finite element model for Haversian bone tissue that includes the main microstructural components (interstitial bone, cement lines, and secondary osteons with separate lamellar bone layers and a Haversian canal);

- To validate the model by comparing predictions with established trends reported in the literature and by conducting a series of experiments measuring mechanical properties as a function of microstructural characteristics;

- To use the model to study, identify, and characterize basic structure/property relations exhibited by bone tissue and formulate ways in which this knowledge can be applied to the development of more advanced aerospace composite materials; and

- To identify and specify further improvements and modifications needed in the model and additional experimental work required for more definitive validation of the model.

RESEARCH DESCRIPTION

Background

Bone is a composite material consisting of both solid and fluid phases. Blood and extracellular fluids comprise the fluid phase. The solid phase is composed primarily of a collagen matrix interspersed with a mineral compound, hydroxyapatite. Bone tissue is generally divided into two types: trabecular, or cancellous, bone and compact, or cortical, bone. Compact bone is much more dense than trabecular bone, which possesses a spongy structure. Three types of compact bone are generally recognized: woven, lamellar, and Haversian (or osteonal). Further details of these distinctions are well documented [1, 2, 3]. Haversian compact bone is the predominant bone type in the mid-shaft region of long bones like the femur and tibia in adult humans. The primary microstructural element of Haversian bone is the secondary osteon, as shown in Fig. 1. The very first osteons formed in growing primary lamellar bone are termed primary osteons. Osteons formed from subsequent remodeling are termed secondary osteons.

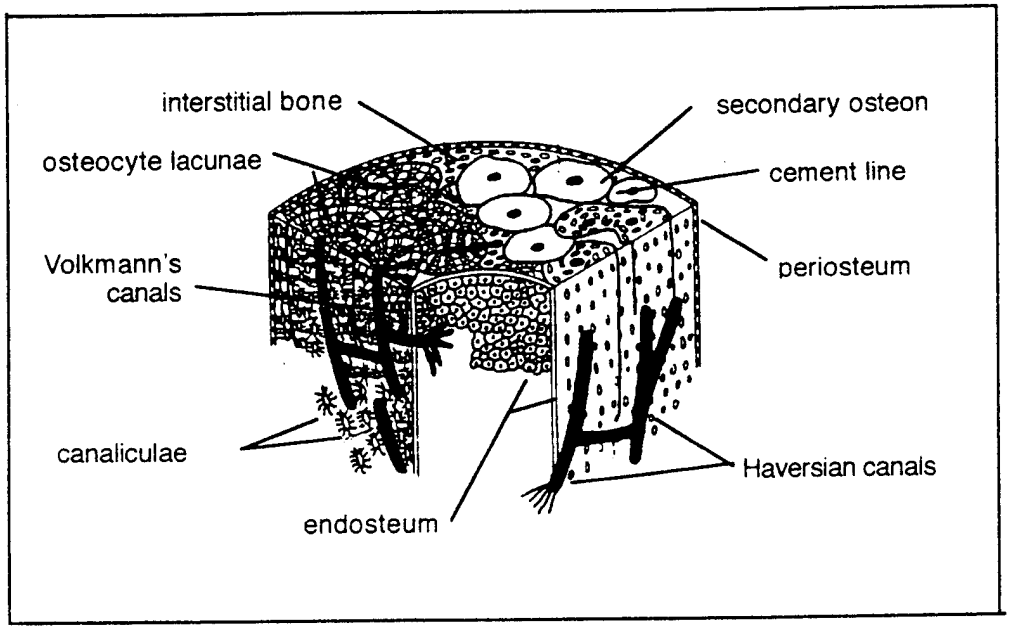

Figure 1. Idealized view of bone mid-shaft showing compact bone microstructure (adapted from [4]).

Osteons are basically cylindrical in shape with diameters ranging from 100μm to 200μm. They are packed rather tightly together and oriented roughly parallel to one another along the axis of the long bone. The sectional view of Fig. 1 exaggerates the relative size of osteons since there are typically 10 to 50 layers of osteons through the wall thickness of the long bone. Osteons are typically composed of 20 to 30 concentric layers of lamellar bone with a hollow center, the Haversian canal. Haversian canals provide passageways for nerves and arteries. Volkmann canals run transverse to the main bone axis periodically connecting adjacent Haversian canals. A

relatively thin (1-5μm) layer of highly mineralized material, called the cement line, surrounds each secondary osteon. The cement line is laid down as bone resorption ends and new bone formation begins. This amorphous 'interphase' material also contains polysaccharides and collagen. Small cavities, called lacunae, contain bone cells and lie between adjacent lamellar bone layers. Lacunae are interconnected with one another and to Haversian canals through tiny passageways called canaliculae. The remaining space between Haversian systems is occupied by less organized 'interstitial' lamellar bone. In mature human bone, this bone tissue is actually composed of fragments of osteons that have been resorbed away (incompletely). Woven bone and primary lamellar bone can also persist as interstitial bone. Mature equine (horse) bone is also predominantly Haversian, but bovine (cow or steer) bone is typically a mix of Haversian and lamellar bone (also called plexiform bone).

The particular type of bone tissue studied in this research is Haversian compact bone tissue because its microstructure resembles that of a fiber reinforced composite material. The fibers in this case, however, are Haversian systems, or secondary osteons. Thus, they are hollow, layered, and surrounded by a distinct 'interphase' fiber/matrix material, known as the cement line. The hollow fibers are furthermore not perfectly straight but in fact spiral slightly and branch. The 'matrix' material is the interstitial bone lying between complete osteons. The matrix is therefore quite similar in composition and properties to the fiber component. A microradiograph of equine Haversian compact bone tissue is shown in Fig. 2.

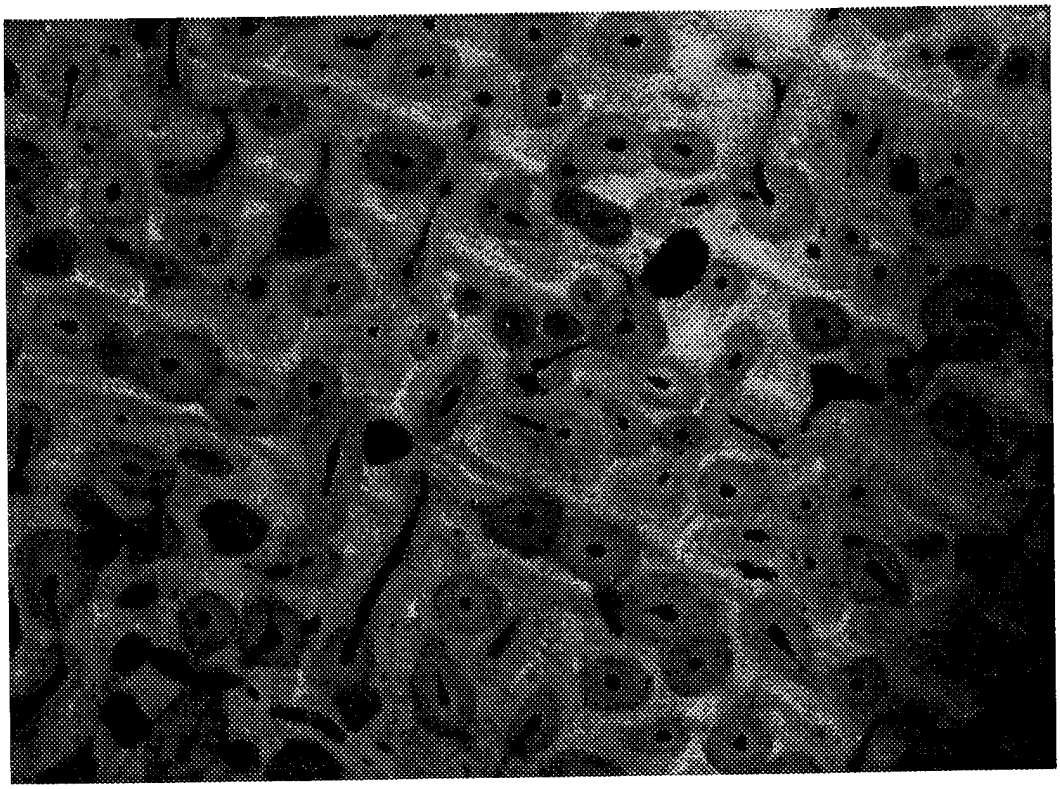

Figure 2. Microradiograph of Haversian compact bone transverse section.

Theoretical Modeling

The underlying strategy in seeking to develop theoretical micromechanics models relating macroscopic mechanical behavior to microstructural details has been to build upon techniques developed for aerospace composites. The two basic methodologies examined are: (1) finite element unit cell analyses, and (2) analytical micromechanics approaches (particularly effective medium methods).

Porosity effects. A two-dimensional finite element model was developed based upon an idealized representation of Haversian compact bone microstructure [5]. The bone microstructure is depicted in Fig. 3. The three solid components are the osteons, interstitial bone, and cement lines, which represent the fiber, matrix, and interphase constituents, respectively. Note as well that the fiber is hollow with the Haversian canal being the only void space represented. Fiber packing geometries have been studied for either a square array or hexagonal array, the latter of which is shown in Fig. 3. A typical mesh generated for this case is shown in Fig. 4. The finite element modeling pre-processor PATRAN was used in conjunction with the ABAQUS finite element solver to analyze this model.

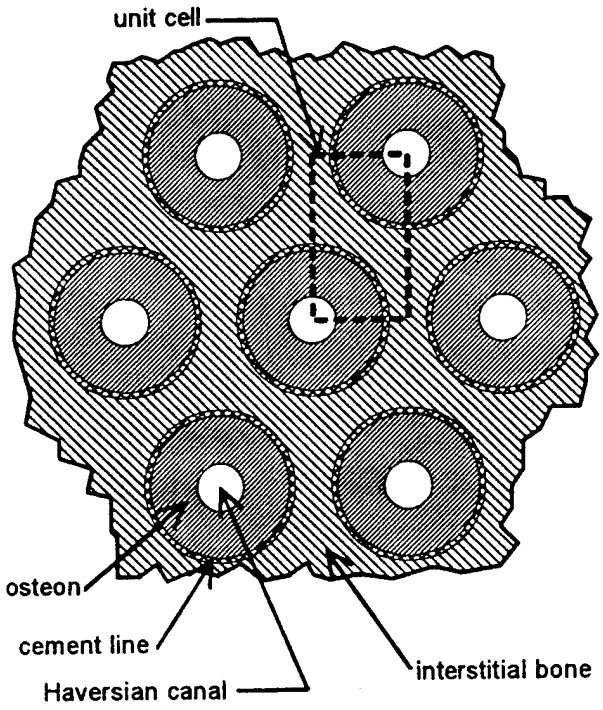

Figure 3. Idealized microstructure of Haversian compact bone.

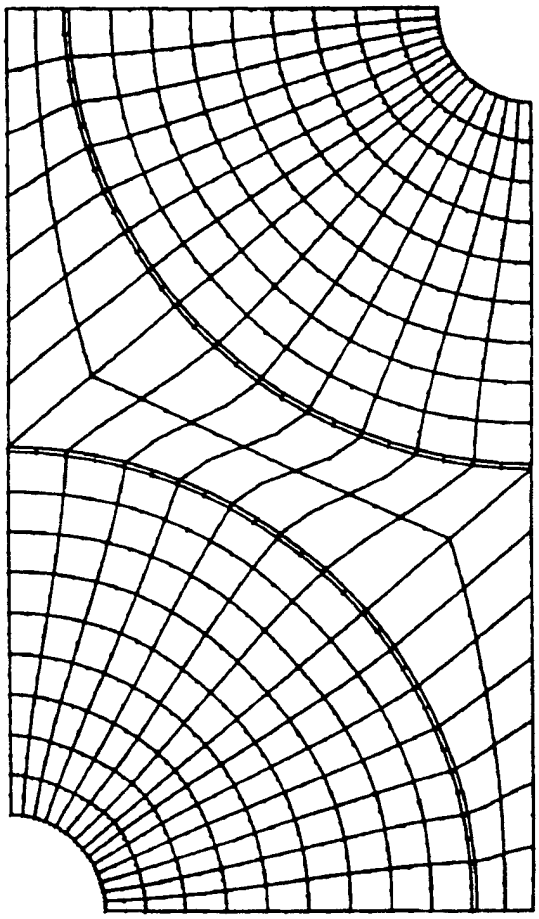

Figure 4. Finite element mesh analyzed.

Baseline mechanical properties used for each constituent are summarized in Table 1. The interstitial bone is taken to be slightly higher in modulus than a typical osteon because it is older than the more recently formed osteons and therefore more highly mineralized. Table 2 compares the hexagonal array results with those generated using a square array. Note that E_{11} is the longitudinal, or axial, modulus whereas E_{22} and E_{33} are moduli in the transverse directions. The Haversian porosity in this case is 3%. Note that the results are essentially the same for hexagonal and square packing with the exception of a slight discrepancy for E_{22}.. In addition, hexagonal packing offers the advantage of being able to model higher fiber volume percentages, so it has been chosen as the method for all subsequent finite element unit cell modeling.

Table 1 - Constituent properties used in micromechanics model

Constituent	E (GPa)	ν
Osteon	12.0	0.3
Cement line	6.0	0.4
Interstitial bone	15.0	0.3

Table 2 - Predicted macroscopic properties for hexagonal vs. square packing geometry

Array	E_{11}	E_{22}	E_{33}	ν_{12}	ν_{23}	ν_{21}
Square	12.3	11.7	11.7	0.30	0.30	0.29
Hexagonal	12.3	11.3	11.3	0.30	0.31	0.28

Note: elastic moduli are in GPa

The Haversian porosity is a parameter which greatly influences the macroscopic material properties of bone and is considered an important variable in micromechanics modeling. In the finite element model, the Haversian porosity is altered by changing the diameter of the Haversian canal, i.e. the inner radius of the hollow fiber. Porosity variations from 3% to 9%, which are reasonable values found in the literature, have been studied. Table 3 details the influence of porosity on transverse and longitudinal moduli as well as Poisson's ratio. The results are baasically as expected: The moduli generally decrease with increasing porosity, and the transverse moduli are more sensitive to porosity variations.

Table 3 - Effect of porosity on macroscopic properties

Porosity (%)	E_{11}	E_{22}	ν_{12}	ν_{23}	ν_{21}
3	12.3	11.7	0.30	0.30	0.29
5	12.2	11.1	0.30	0.29	0.28
7	11.9	10.6	0.30	0.29	0.27
9	11.6	10.1	0.30	0.28	0.26

Note: elastic moduli are in GPa

The Mori-Tanaka effective medium method of estimating the overall mechanical properties of a fiber reinforced composite has been extended to allow for porosity by Zhao, et al. [6]. Even though experimental data is limited, they report reasonable predictions for variations in mechanical properties as a function of porosity. The simplest case to consider as a model for Haversian compact bone is that of 'needle-shaped' voids representing the Haversian canal. That is, the voids are long and slender, parallel to one another, and aligned with the overall longitudinal axis. The variation in longitudinal modulus with porosity is linear in this case, however, whereas experimental data suggests a power law relation [7]. More plausible comparisons with experimental data are nevertheless possible by using the Mori-Tanaka method for 3-D ramdomly oriented spheroidal voids with appropriate aspect ratios. Results are shown in Fig. 5 for several aspect ratios. The ratio of the longitudinal modulus to the modulus of the solid phase (E_{11}/E_0) is plotted versus porosity. The aspect ratio (a) of 10 represents a prolate spheroidal void and the

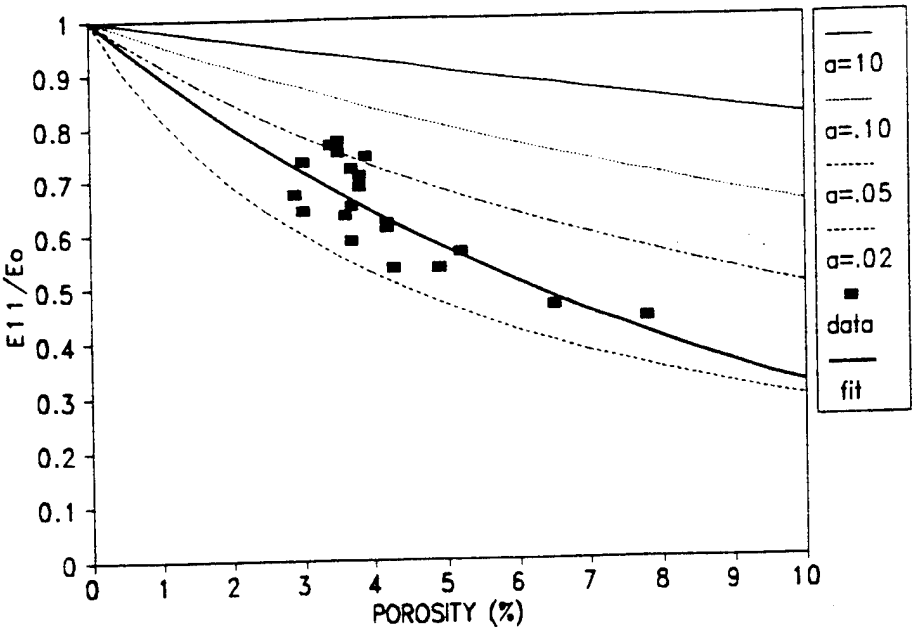

Figure 5. Longitudinal modulus vs. porosity for needle-shaped voids.

other three aspect ratios (.10, .05, .02) represent various oblate spheroidal voids. Prolate voids are more 'rod-like', while the oblate voids are more 'disk-like'. The power-law expression used to fit the experimental data is given by:

$$E = 33.88(1-P)^{10.92} \quad \text{(in GPa)}$$

The curves in Fig. 5 that best fit the data are for oblate voids. This certainly does not describe the shape of the Haversian canal, but the experimental data is for bovine bone, which contains both Haversian and plexiform types of compact bone. No experimental data was previously available for modulus versus porosity for exclusively Haversian compact bone, so the experiments conducted as part of this research have specifically targeted this need.

Most attempts to develop analytical expressions relating porosity and mechanical properties of various engineering materials have resulted in empirical correlations based upon extensive experimental data. These expressions typically take the form of power law relations with particular coefficients and exponents for different materials. In a similar vein, Bert [8] developed a semi-empirical approach combining theoretical and empirical considerations. Cylindrical or spheroidal voids can be modeled with square or hexagonal array spacings. Elastic modulus predictions are compared in Fig. 6 for the finite element unit cell analysis, Mori-Tanaka methods, and the semi-empirical method of Bert. The Mori-Tanaka predictions are for the case of needle-shaped voids. The moduli values are normalized by dividing by the elastic modulus of the solid phase. All three approaches yield the same results for the elastic modulus in the axial direction, i.e. along the main longitudinal axis of the long bone. The cylindrical voids are also aligned with this axis so the decrease in modulus is linear and proportional to the porosity. The elastic modulus transverse to the longitudinal axis is more sensitive to changes in porosity. The results for Bert's model are for a hexagonal array of cylindrical voids and show a slightly greater decrease in modulus with porosity than the other two approaches. The rate of decrease, however, is greatest for the finite element results.

The degree of anisotropy predicted by the models is shown by plotting the ratio of the axial modulus to the transverse modulus. Bert's model predicts greater anisotropy due to the lower transverse modulus values. The ratio increases from approximately 1.0 to 1.35 for Zhao et al. and the finite element model, but reaches a maximum of 1.55 for Bert. These are generally lower than typical ratios reported for human compact bone. Cowin [9] summarized data from four sources which yield the following ratios: 1.48, 1.46, 2.66,

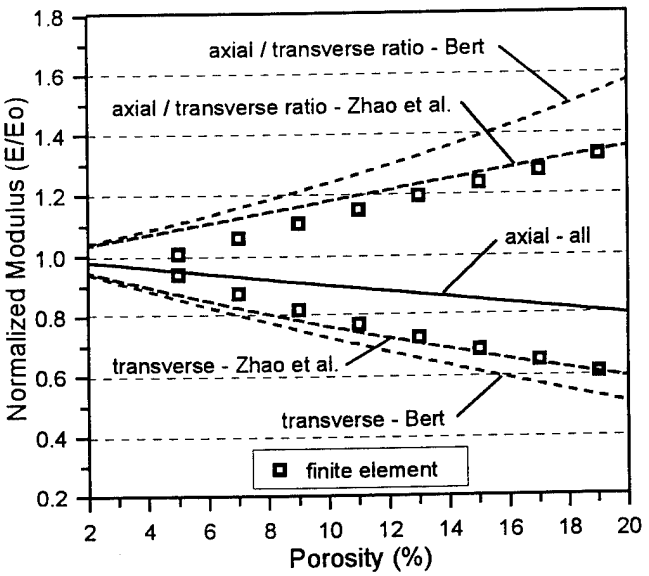

Figure 6. Predictions of modulus vs. porosity.

2.16, 1.67, 1.49. Six values are included because two of the studies found the bone to be orthotropic so two different transverse moduli were reported. None of the studies included any microstructural information about the specimens tested so the porosities are not known. An important point to consider as well is that the two analytical approaches assume the solid phase to be homogeneous and isotropic. Each component of the solid phase in the finite element model is likewise treated as isotropic. The observed degree of anisotropy is likely due in part to the microstructural architecture of the solid phase as well as the presence of voids. The theoretical models nevertheless clearly demonstrate that a significant portion of the anisotropy of Haversian compact bone can be attributable to porosity.

Cement line effects. As mentioned previously, a somewhat mysterious substance known as the cement line separates osteons from the surrounding interstitial bone. The exact mechanical properties (modulus and Poisson's ratio) of the cement line are not known from experimental testing and can only be inferred from indirect testing and from the observed composition of the substance. It is generally believed that the cement line is more compliant [10] than either the osteon or the interstitial bone and that it may in fact be viscous in nature [11]. Moreover, the precise role of the cement line in determining the macroscopic mechanical behavior of compact bone is not known and much debated. Accordingly, cement line modulus values ranging widely (6.0 to 0.12 GPa, or, 50% to 1% of the osteon modulus) have been modeled and the resultant macroscopic properties documented. The thickness of the cement line was also varied from 1.4μm to 5.0μm since it is reported to be between 1μm and 5μm [12]. The effects of these changes on macroscopic properties are shown in Table 4 (1.4μm cement line) and Table 5. As expected, the cement line affects the transverse moduli (E_{22}) much more than the longitudinal moduli (E_{11}). The transverse moduli are particularly sensitive to cement line thickness. Another interesting observation is that these results suggest that the cement line modulus is most likely not as low as 0.12 GPa (i.e. 1% of the osteon modulus), because the macroscopic transverse modulus is lower (6.38 & 3.66 GPa) than generally observed experimentally. Furthermore, the longitudinal modulus results are essentially the same as given by a rule-of-mixtures (uniform strain) approach. The cement line is a very small percentage of the total solid phase components (ranging from 1.7% to 8.6%), so the variation in the longitudinal modulus with cement line properties and thickness is minimal.

Table 4 - Effect of cement line modulus on macroscopic properties

E_{cl} (GPa)	E_{11}(GPa)	E_{22}(GPa)	ν_{23}	ν_{21}
6.0 (50%)*	12.3	11.5	0.31	0.28
3.6 (30%)	12.1	11.3	0.31	0.28
1.2 (10%)	11.9	10.4	0.33	0.26
0.12 (1%)	11.6	6.38	0.36	0.16

* percent of osteon modulus

Table 5 - Effect of cement line thickness on macroscopic properties

E_{cl} (GPa)	E_{11} (GPa)		E_{22} (GPa)		ν_{23}		ν_{21}	
	1.4μm	5.0μm	1.4μm	5.0μm	1.4μm	5.0μm	1.4μm	5.0μm
6.0 (50%)*	12.3	11.8	11.5	10.9	0.31	0.32	0.28	0.29
3.6 (30%)	12.1	11.6	11.3	10.3	0.31	0.33	0.28	0.27
1.2 (10%)	11.9	11.4	10.4	8.53	0.33	0.36	0.26	0.23
0.12 (1 %)	11.6	11.3	6.38	3.66	0.36	0.35	0.16	0.10

* percent of osteon modulus

Analytical effective medium approaches can also be adapted to more realistically model the solid portion of the bone microstructure as distinct components (osteon, cement line, & interstitial bone) rather than as a single phase. The work of Dasgupta and Bhandarkar [13] considers the Mori-Tanaka technique for the case of a fiber surrounded by one or more 'interphases' embedded in a matrix material. This model has been employed for the case of Haversian cortical bone by regarding the Haversian canal as the fiber (modulus approximately zero) with the osteon and cement line as two interphase materials. Results from this approach are compared with those of the finite element unit cell analysis in Fig. 7. The ratios of the longitudinal modulus to the transverse modulus are plotted vs. cement line modulus for two cement line thicknesses. The two methods match well for higher cement line moduli, but the Mori-Tanaka approach seriously underestimates the transverse modulus otherwise. The modulus ratios plotted provide an indication of the degree of anisotropy in the macroscopic modulus predictions and the effects of the cement line upon these. The longitudinal modulus is only 10 to 20 percent higher than the transverse modulus for cement line moduli of 50% and 30% of the osteon modulus. As the cement line modulus further decreases, however, the ratio increases rather dramatically, particularly for the thickest (5mm) cement line. Overall, these ratios are lower than those typically reported in the literature. As noted previously, Cowin's [9] summary yields the following ratios: 1.48, 1.46, 2.66, 2.16, 1.67, and 1.49.

At least two views are possible when comparing the modeling results with experimental data. One is that the model simply lacks sufficient realism in its present form because it predicts a much lower modulus ratio for most of the range of parameters studied. In this case, other sources of anisotropy may need to be included in the model. Prominent among these would be to consider the osteon to be anisotropic due to the preferential orientation of collagen and apatite in the concentric layers of osteonic lamellar bone. This can be modeled explicitly within the framework of the present approach but the precise degree of anisotropy of the osteon is unknown. This becomes to a large extent then another adjustable parameter that can be varied over a wide

range as needed. Osteon anisotropy has been investigated theoretically [14,15], but no direct experimental evidence is currently available to firmly establish anisotropic osteon properties.

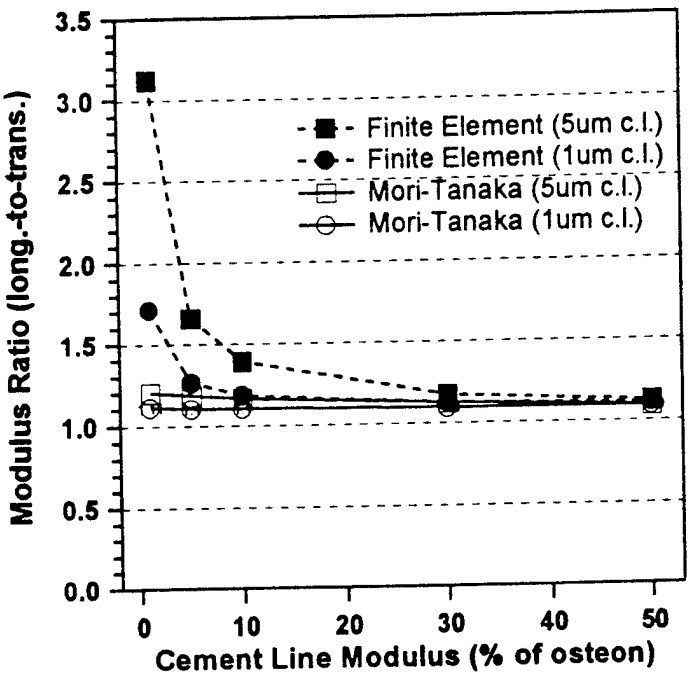

Figure 7. Cement line effects on degree of anisotropy.

Another view is that the lower cement line modulus cases in the present analysis more accurately reflect the true nature of the cement line and this is why the predictions match the experimental data more closely for these cases. The current model treats the cement line as perfectly bonded to the surrounding bone, which may therefore overstiffen the model relative to the actual physical situation. The lowest cement line modulus values of 5% and 1% could be considered somewhat unrealistic since they are 20 and 100 times, respectively, lower than the osteon modulus, but the net effect taken together with the perfect bonding assumption may in fact combine to produce a response quite close to the actual case (because of slip or viscous behavior). In either case, the overriding need is for more definitive experimental data on the mechanical properties of the osteon and the cement line. Such information will not be easy to come by, however, and these results demonstrate the utility of micromechanics modeling in exploring the possible effects of microconstituent properties on macroscopic properties. Specifically, the results herein suggest that the cement line is likely a significant contributor to Haversian compact bone anisotropy. The macroscopic anisotropy in Haversian bone mechanical properties is not necessarily due solely to osteon anisotropy and can conceivably be explained based upon cement line properties alone. These possibilities should therefore remain open to inquiry until direct experimental evidence indicates otherwise.

Experimental Testing

The experimental portion of this research has taken several forms in an attempt to characterize macroscopic mechanical properties and their relation to microstructural details. The most comprehensive testing has been ultrasonic through-transmission testing to measure the anisotropic elastic moduli. Tensile testing to failure has also been conducted to determine elastic modulus (longitudinal direction only) and tensile strength. Dynamic mechanical testing has also been initiated in order to measure viscoelastic moduli and damping properties. All testing has been folllowed by extensive microstructural analysis in order to quantify various features of the bone tissue microstructure. A working arrangement has been developed between the project and several laboratories in order to establish an experimental protocol for specimen acquistion, storage, machining, and testing. Fresh equine bone samples are obtained from the necropsy lab in the Department of Veterinary Physiology and Pharmacology at Texas A&M University. Sections of the middle portion of the cannon bone were cleaned and cut to lengths of approximately 2½ inches. The specimens were kept frozen until further cutting. They are then rough cut into quarters and placed in Ringer's solution and refrigerated. A low speed diamond blade wafering saw was used next to cut test specimens to dimensions appropriate for the particular test method.

Ultrasonic testing. The mathematical model for estimating mechanical moduli by ultrasound is constructed by substituting the expression for a bulk wave into the Navier equation from linear elasticity. The substitution gives three equations, which form an eigenvalue problem with the terms ρv^2 as roots. A set of roots can be found after specifying the direction cosines for a given plane wave. Once the roots for a particular set of direction cosines are found, the direction of displacement is given by substituting each of the roots back into the set of matrix equations. Repeating the process for all the possible pairs of direction cosines yields the following relations between velocities, density(ρ), and stiffness coefficients (C_{ij}):

$$\rho v_{1,1}^2 = C_{11} \quad \rho v_{2,2}^2 = C_{22} \quad \rho v_{3,3}^2 = C_{33}$$

$$\rho v_{2,3}^2 = C_{44} \quad \rho v_{3,2}^2 = C_{44}$$

$$\rho v_{1,3}^2 = C_{55} \quad \rho v_{3,1}^2 = C_{55}$$

$$\rho v_{1,2}^2 = C_{66} \quad \rho v_{2,1}^2 = C_{66}$$

$$C_{12} = -C_{66} + \sqrt{-C_{11} - C_{66} + 2\rho v_{12,12}^2}\sqrt{-C_{22} - C_{66} + 2\rho v_{12,12}^2}$$

$$C_{13} = -C_{55} + \sqrt{-C_{33} - C_{55} + 2\rho v_{13,13}^2}\sqrt{-C_{11} - C_{55} + 2\rho v_{13,13}^2}$$

$$C_{23} = -C_{44} + \sqrt{-C_{33} - C_{44} + 2\rho v_{23,23}^2}\sqrt{-C_{22} - C_{44} + 2\rho v_{23,23}^2}$$

These relations are for the more general case of orthotropic material behavior. The velocities $v_{i,i}$ are for longitudinal waves and $v_{i,j}$ are for shear waves. The velocities denoted $v_{ij,ij}$ are 'quasi-velocities' measured along axes 45° to the three orthotropic axes. For transversely isotropic material behavior, only one of these quasi-velocities must be measured. All of the velocities in the model are assumed to be phase velocities. Phase velocity is the velocity of a point of constant phase, whereas group velocity is the velocity at which energy travels through the material. The two are not equal for a dispersive material, but Ashman [16] has shown compact bone to be only mildly dispersive so group velocity should be a reasonable estimate of true phase velocity. This is important for the present study since group velocity is typically measured by ultrasonic transducers. The engineering properties can be obtained by inverting the stiffness matrix C_{ij} to get compliance terms S_{ij} and performing simple algebra.

The ultrasonic testing protocol is summarized in Fig. 8. The sonic velocities of longitudinal and shear waves were determined for each specimen using a through transmission approach. The classical technique of measuring travel time and specimen thickness was used to calculate the velocities. Pulse transducers with a nominal frequency of 5 MHz were used for both longitudinal and shear waves. One longitudinal and two shear velocities were measured along each of the three orthogonal axes of the cube specimen. Following this, a pair of oblique faces were cut at a 45° angle to the overall long axis of the bone (the 3-axis). Three 'quasi-velocities' were then measured along this axis to complete the data needed to calculate the tranversely isotropic properties. All specimens were tested wet. A paired cube immediately adjacent to the test cube was cut and embedded for microstructural analysis.

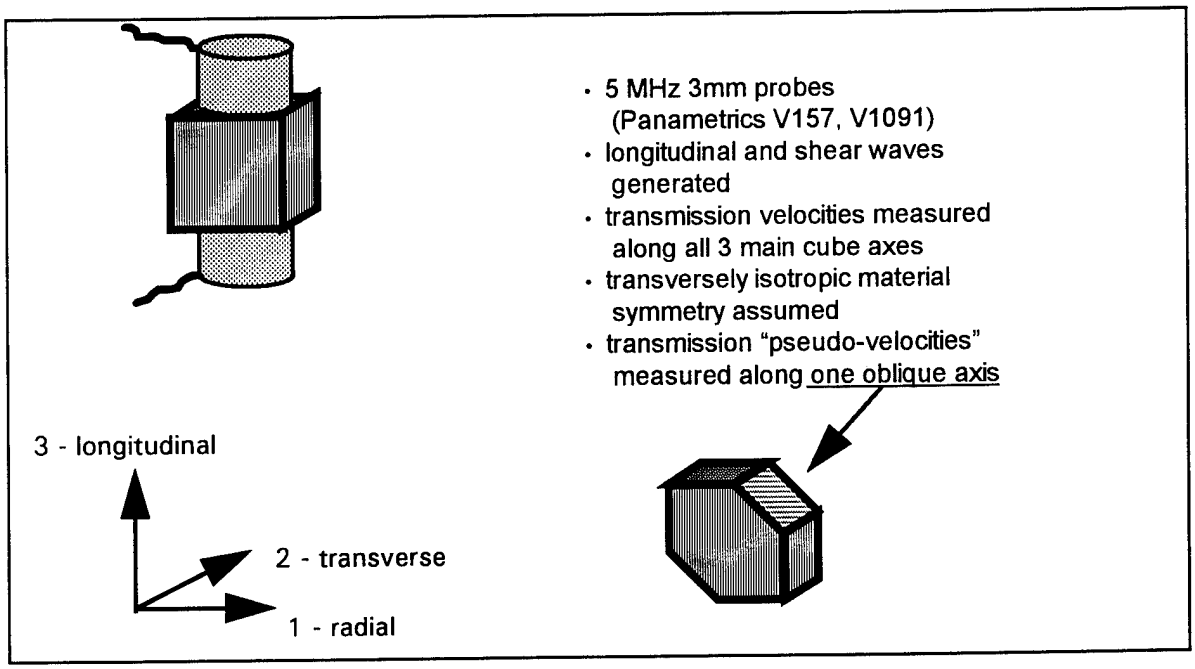

Figure 8. Ultrasonic testing details.

Tensile testing. Specimens for tensile testing were first cut into 'slabs' measuring approximately 2"x 3/8"x1/8" on a low speed diamond wafering saw under continuous irrigation with water. The long dimension is aligned with the long axis of the bone. These slabs were then submitted to the Testing, Machining, and Repair Facility of the Texas Engineering Experiment Station for machining into standard 'dogbone' shaped tensile specimens (see Fig. 9). The machining is done at low speed and constant irrigation with distilled water. Once machined, each specimen is stored in a separate vial of Ringer's solution and refrigerated until tested. Testing must follow in less than 90 days or the specimens should be refrozen. Custom extensometers were obtained for measuring the extension of the gage section. The specimens were mounted in an Instron servo-controlled mechanical testing machine in articulating grippers to prevent unintended bending loading. Quasi-static tensile loading was applied in stroke control at a cross-head displacement rate of 0.2"/minute. A sample stress-strain curve is presented in Fig. 10. The elastic modulus is calculated from the slope of a regression line fit to the linear portion of the curve, and the tensile strength is taken to be the maximum stress reached during the test.

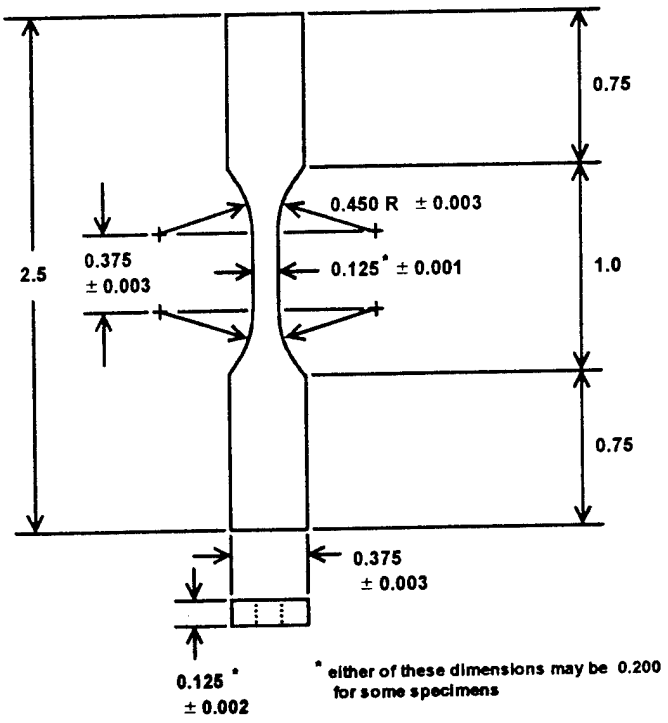

Figure 9. Tensile test specimen (all dimensions in inches).

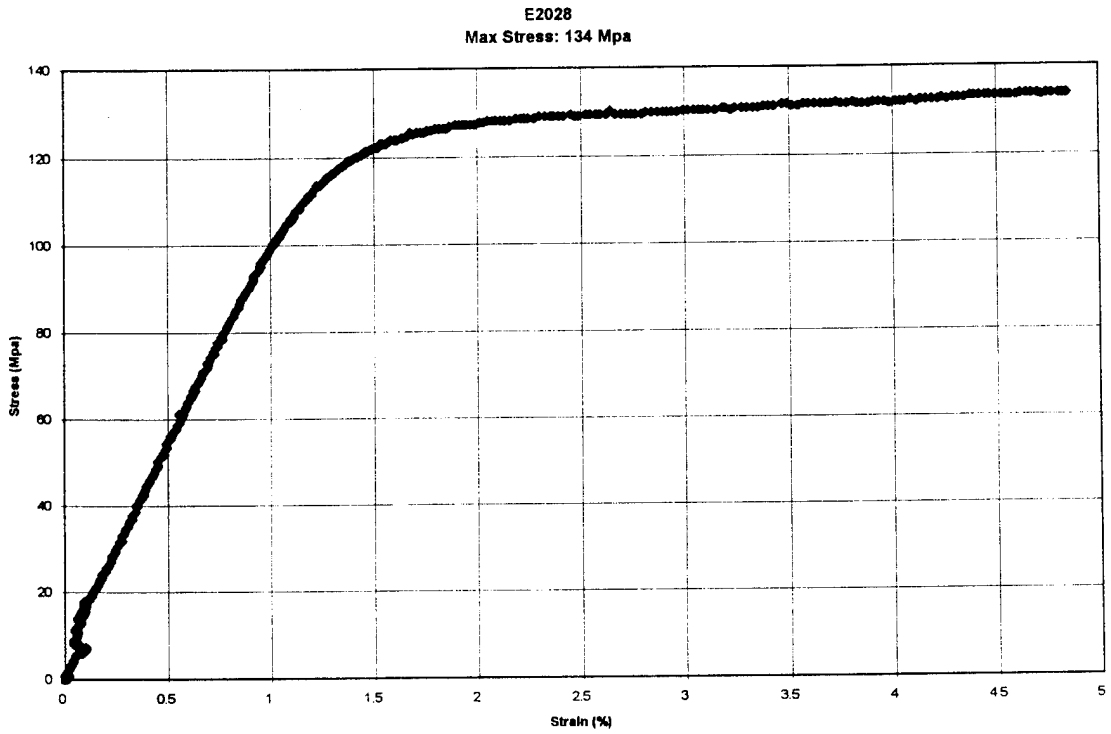

Figure 10. Typical stress-strain curve from tensile testing.

Dynamic mechanical testing. Dynamic mechanical testing is commonly employed for measuring the viscoelastic behavior of polymeric materials. While there are many different tests available for characterizing the viscoelastic behavior of materials, such as creep and relaxation tests, the dynamic mechanical test procedure focuses on the upper boundary of the frequency spectrum. In a dynamic mechanical test, an oscillatory, or periodic, strain and the resulting load and stress are measured. In the current work torsional loading was applied, in which case the input strain has the following form:

$$\gamma = \gamma_o Sin(\omega t)$$

where γ_o is the maximum strain amplitude and ω is the angular frequency in radians per second. For linear viscoelastic behavior, when equilibrium is reached the shear strain and shear stress both vary sinusoidally, but the stress lags behind the strain. The resulting output for strain-controlled loading is a shear stress of the following form:

$$\tau = \tau_0 Sin(\omega t + \delta)$$

where τ_o is the amplitude of the shear stress. The phase lag between the shear stress and applied shear strain is given by δ. The phase lag ranges from 90° for a purely viscous material, to 0° for a purely elastic material. In a dynamic mechanical test, τ and γ are related by:

$$\tau = \gamma_o G^* = \gamma_o [G' \sin(\omega t) + G'' \cos(\omega t)]$$

where G* is the complex modulus, and G' and G" are defined as the storage modulus and loss modulus, respectively, and are given by:

$$G' = \frac{\tau_o}{\gamma_o} \cos\delta$$

and

$$G'' = \frac{\tau_o}{\gamma_o} \sin\delta$$

The loss factor, or *tan* δ, can then be expressed as a function of G' and G":

$$\tan\delta = \frac{G''}{G'}$$

It is then obvious that as the phase angle approaches zero, the storage modulus approaches the elastic modulus and the loss modulus goes to zero. In dynamic mechanical analysis with torsional loading, a specified sinusoidal rotation is applied to one end of the specimen. The test machine measures the torque at the other end of the specimen, as shown in Fig. 11, and the phase difference between the stress and strain.

Dynamic mechanical testing was conducted on a Rheometrics RDS II located in the Polymer Technology Center at Texas A&M University. Specimens for dynamic mechanical testing consisted of slabs approximately 2"x 3/8"x1/8" in size. Preliminary tests were conducted to determine an appropriate strain amplitude and frequency range for linear viscoelastic behavior. Specimens were stored in Ringer's solution and refrigerated until just prior to testing. They were then allowed to reach room temperature but maintained moist. Immediately before mounting in the testing machine, each specimen was coated with a thin layer of high vacuum silicone grease to prevent moisture loss during testing. The torsional strain amplitude was 0.015% and the frequency was varied over three decades from 0.1 to 100 rad/s. Each test took roughly 10 minutes. Results are reported as storage modulus (G'), loss modulus (G"), and loss factor (tan δ) as a function of frequency. A typical set of plots is shown in Fig. 12.

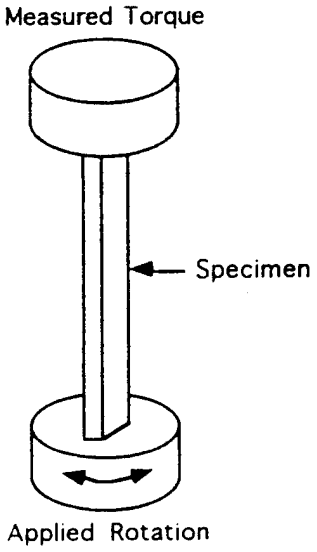

Figure 11. Schematic of dynamic mechanical testing method.

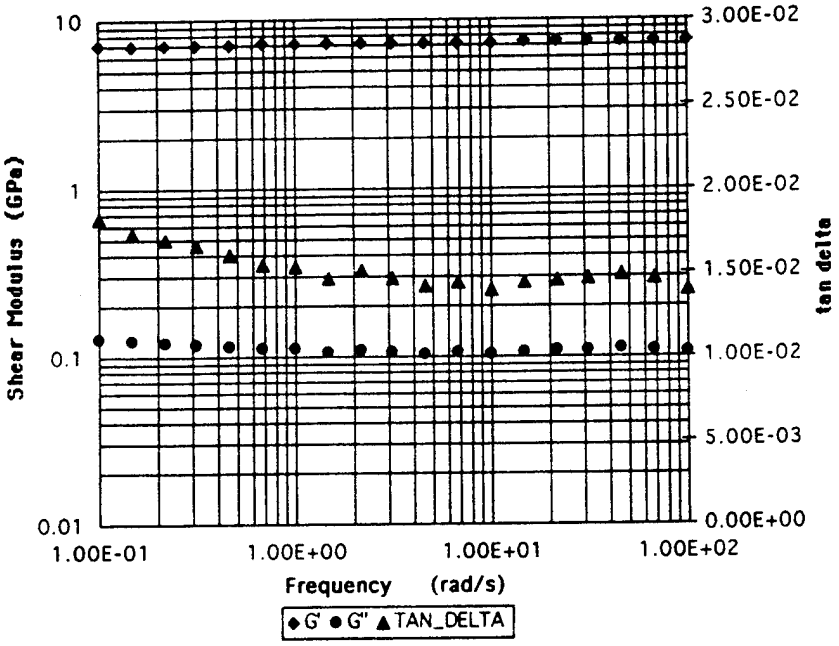

Figure 12. Typical results from dynamic mechanical tests.

Microstructural analysis. Specimens from all three testing types were analyzed for microstructural details. Quantitative characterization of the microstructure can be grouped into two general categories: (1) physical properties, such as densities and mineralization; and (2) image analysis of microradiographs of transverse sections.

The first quantity measured was the bulk density -- the average of the bone composition, water content, and void spaces. A method based upon Archimedes' Principle allows the wet density to be determined by the following relation:

$$\rho_{bone} = \left(\frac{W_{moist}}{W_{moist} - W_{susp}} \right) \rho_{water}$$

where, ρ_{bone} is the bulk wet density of the specimen, W_{moist} is the weight of the moist specimen, W_{susp} is the weight of the specimen when it is suspended with wire in distilled water, and ρ_{water} is the density of distilled water. An analytic balance was used to weigh the specimens with a precision of five decimal places when measuring grams. The dry density was determined next. The volume of the section was calculalted the wet density calculations, since the density and wet weight are known, and also measured mechanically using a digital caliper. The specimens were placed in pyrex beakers and dried in a convection oven at 60°Celsius for about two days. The specimens were then weighed again using the analytic balance by weighing the specimen and beaker, together, then subtracting the weight of the beaker, thus giving the weight of the dried specimen. The dry density was then be computed as the ratio of the dry weight to the volume of the specimen:

$$\rho_{dry} = \frac{W_{dry}}{V}$$

where, W_{dry} is the dry weight of the specimen, while V is the volume of the specimen.

Another microstructural parameter measured was the mineral content for each specimen. In order to quantify the mineral content, the specimen must first be ashed. This process involved cooking the specimens (in their pyrex beaker with crucible lids covering) at 600°C for 24 hours in order to burn off all other material, thus reducing the bone to its mineral phase. This remaining "ash" is composed of a combination of calcium crystals, phosphorus, and other trace materials. The specimens were then weighed again on the analytic balance after the oven was allowed to cool to room temperature. Cooling the specimens is crucial because the mass will fluctuate until the specimens reach room temperature. The % mineralization is then calculated as the ratio of the weight of the remaining ash material to the dry weight of the whole specimen:

$$\%Mineralization = \left(\frac{W_{ash}}{W_{dry}} \right) * 100$$

where, W_{dry} is the dry weight of the specimen, and W_{ash} is the weight of the ash material of the specimen. This quantity is also called the "ash weight" in the literature, or "ash weight %", even though the units are a simple percentage.

Microradiography and image analysis were conducted through subcontract arrangements with the University of Texas Medical Branch (UTMB) at Galveston. Samples from each test specimen were cut and imbedded in Buehler Castolite Resin. Next, a 100 micron thick slice was cut using an Isomet saw. A microradiograph was then taken using a 10 kilovolt, 20 millamp Sorensen x-ray system, with an exposure time of approximately 10 minutes. Fig. 12 shows a

sample microradiagraph taken of a section. The porous portions of the bone specimen microradiographed are indicated by the darkest regions. Conversely, the most highly mineralized portions of the bone are illustrated by the regions with the lightest colors. The porosity of the bone tissue in each microradiograph image was using Optimas 4.2 image analysis software. Threshold levels were adjusted manually until all 'dark' regions were highlighted and then the percent area of the highlighted pixels was calculated. Each field is 1 mm^2 in area. The number of fields analyzed for each specimen varied with specimen size. The number of fields analyzed was 9 for the specimens from ultrasonic testing, 5 from the tensile specimens, and 8 from the specimens from the dynamic mechanical testing. Results were then averaged for all fields analyzed. Other microstructural parameters of interest were the extent of cement line material present and the area fraction of the cross-section occupied by Haversian systems (osteons). These were not calculated for all cases because the procedures are much more labor intensive. In this case, the outer boundaries of each osteon in the field was traced manually using the 'mouse' on the PC. The total length of the lines traced was then calculated by the image analysis software. The length was then normalized by dividing by the total area of the field (1 mm^2) to give a cement line 'density' (in units of mm/mm^2). The area enclosed by each closed curve was also calculated and the percent osteon area determined as this quantity divided by the total area of the field (1 mm^2).

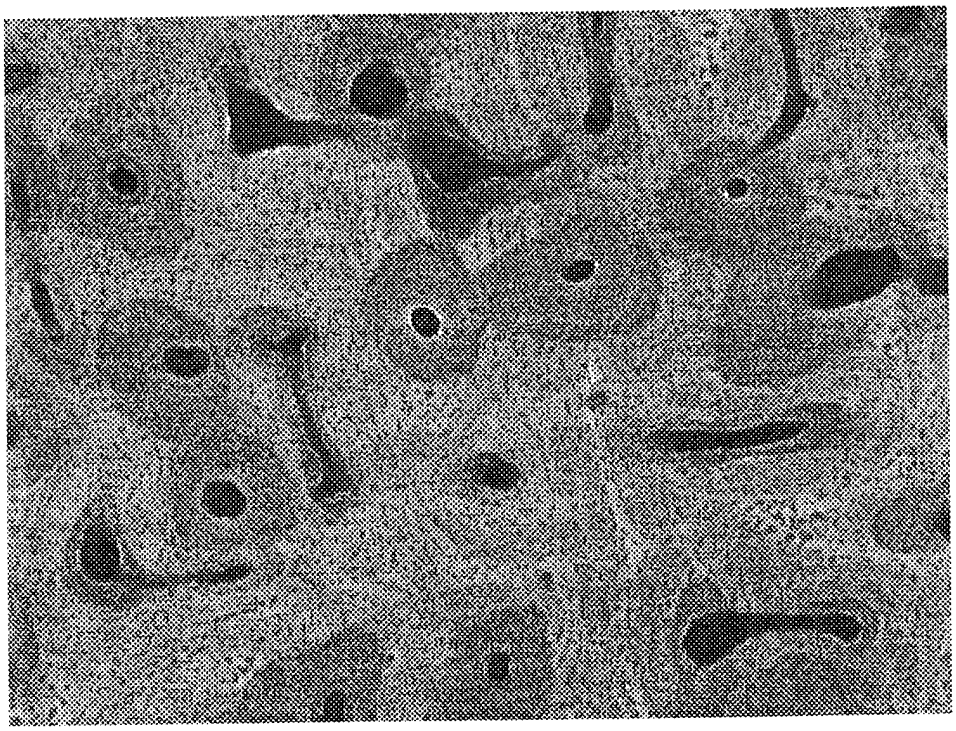

Figure 12. Sample microradiograph of bone section (63X).

Properties vs. Microstructure

In order to gain insight into trends and effects, results from all three modes of mechanical testing were analyzed and plotted versus various microstructural parameters.

Anisotropic moduli. The main results from the ultrasonic tests were a full set of anisotropic moduli (and Poisson's ratios) for each specimen, assuming transversely isotropic material symmetry. The variation in longitudinal and transverse elastic moduli with porosity is depicted in Fig. 14. The trends are as expected, with moduli generally decreasing with increasing porosity. No data has been previously reported for variation in transverse modulus with microstructure, so the longitudinal modulus alone is compared with other experimental results in Fig. 15. Note that the data of Schaffler and Burr [7] has been divided into osteonal and plexiform tissue types. The dashed line representing a linear regression is fit only to the osteonal results for more direct comparison with the present results. Data from a recent study by McCalden, *et al.* [17] is also included (but only plotted for the same range of porosities as the current work). Further, these results were generated by manually cross-plotting modulus vs. porosity from two separate graphs of modulus vs. age and porosity vs. age as presented in the original paper. The regression line for the present study has a slope between the other two data sets. An unexpected feature of the present results (Fig. 14) is that the transverse modulus appears to be less sensitive to variations in porosity than the longitudinal modulus. This is contradictory to what would be expected based upon an idealized theoretical treatment of porosity as parallel hollow cylindrical voids. The theoretical results presented previously are compared to the current experimental results in Fig. 16. The theoretical results show that both the longitudinal (E_{33}) and transverse (E_{22}) moduli do indeed decrease with porosity, but the ratio E_{33}/E_{22} increases with porosity highlighting the greater sensitivity in E_{22}. This confounding finding suggests that such a simplified view of the architecture of Haversian canals (and other void spaces as well) may be inadequate.

The variation in shear moduli with porosity is summarized in Fig. 17. Again, both sets of moduli generally decrease with increasing porosity, as would be expected. These results also show, however, that the sensitivity to variations in porosity is not the same for the 'out-of-plane' shear moduli (G_{13} , G_{23}) and the 'in-plane' shear moduli (G_{12}). Specifically, the larger (negative) slope for the out-of-plane moduli indicates greater sensitivity to porosity. Plots showing the variation in elastic moduli and shear moduli with percent ash weight are given in Figs. 18 and 19, respectively. All moduli generally increase as ash weight increases, but the longitudinal modulus is more sensitive than the the transverse modulus and the out-of-plane shear modulus is more sensitive than the in-plane shear modulus. Similar plots are included for the variation in moduli with osteon area fraction and cement line perimeter in Figs. 20-23. These results are consistent with previous qualitative observations that secondary osteons tend to decrease the modulus and strength of compact bone tissue [18-20]. The continual remodeling that produces secondary osteons would be expected to increase both the osteon area fraction as well as the cement line perimeter. Once again, the longitudinal modulus and out-of-plane shear modulus show greater sensitivity to microstructural variation, increasing osteon area fraction and cement line perimeter in this case.

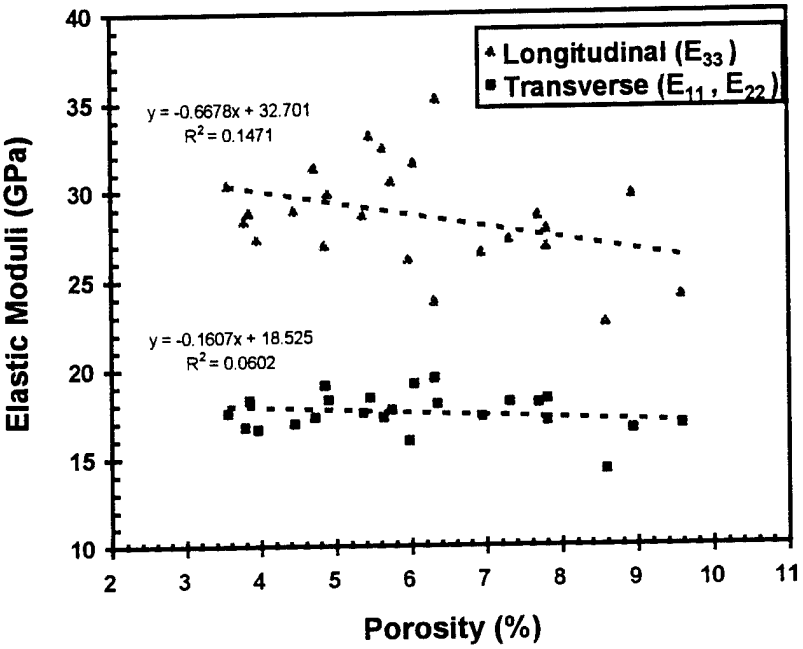

Figure 14. Elastic moduli vs. porosity.

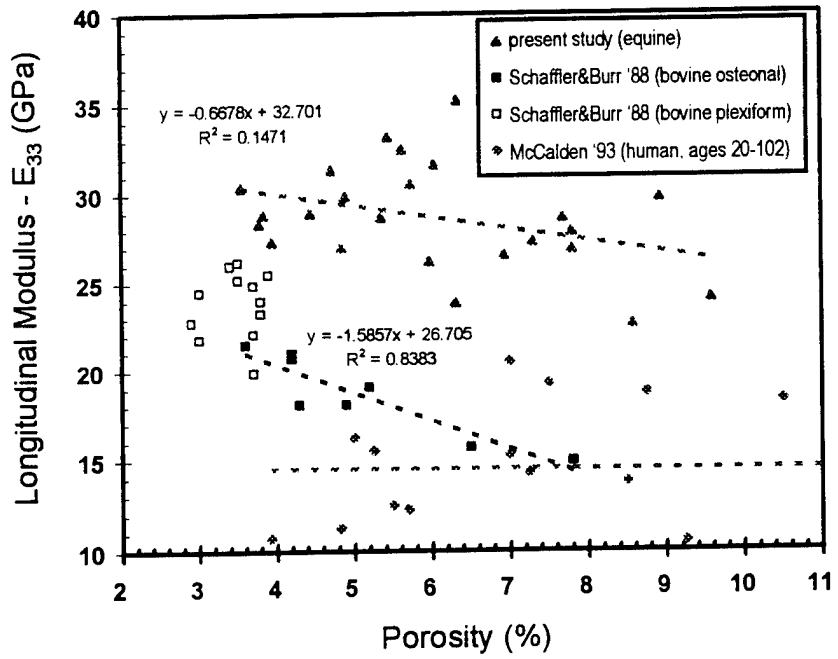

Figure 15. Comparing longitudinal modulus variation with others.

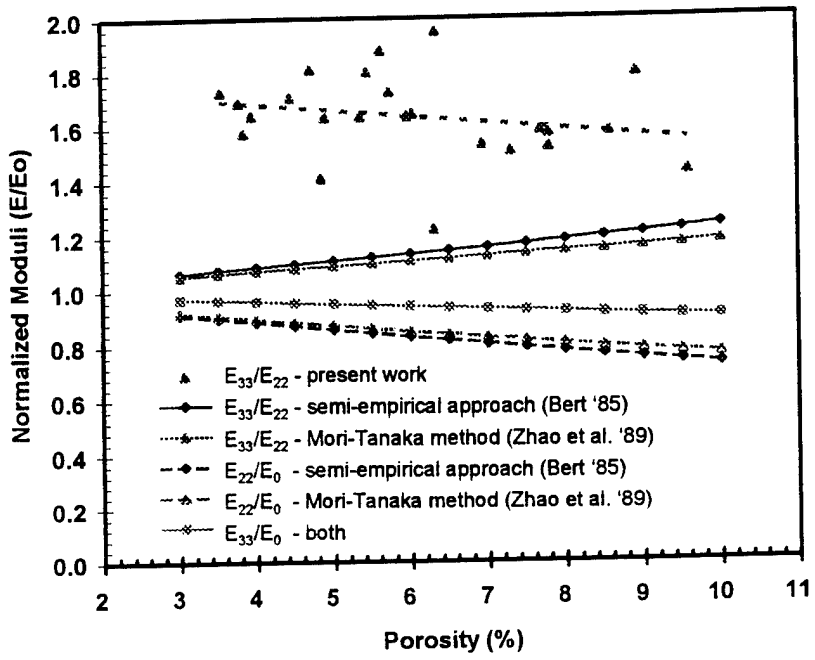

Figure 16. Experiment vs. theory for normalized moduli.

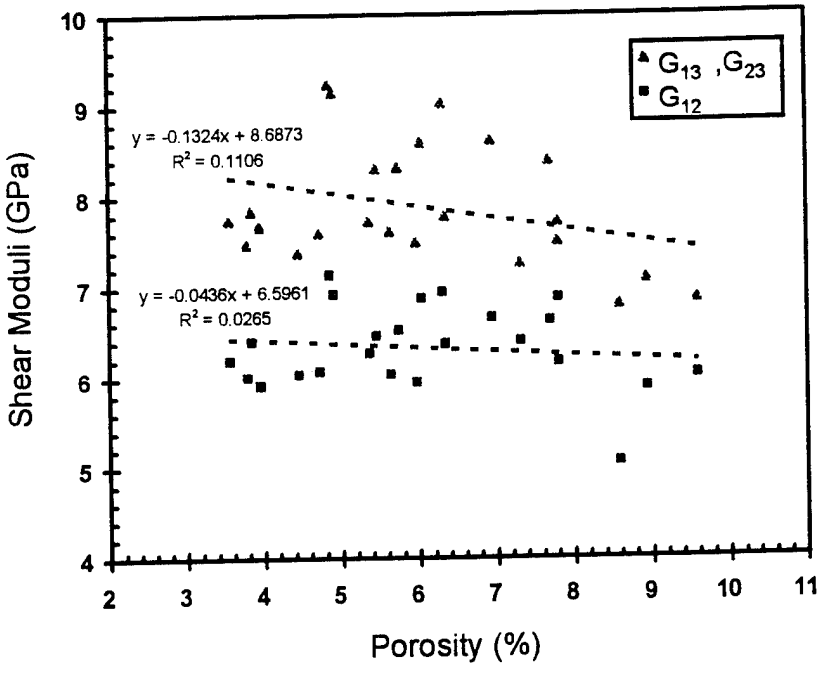

Figure 17. Shear moduli vs. porosity.

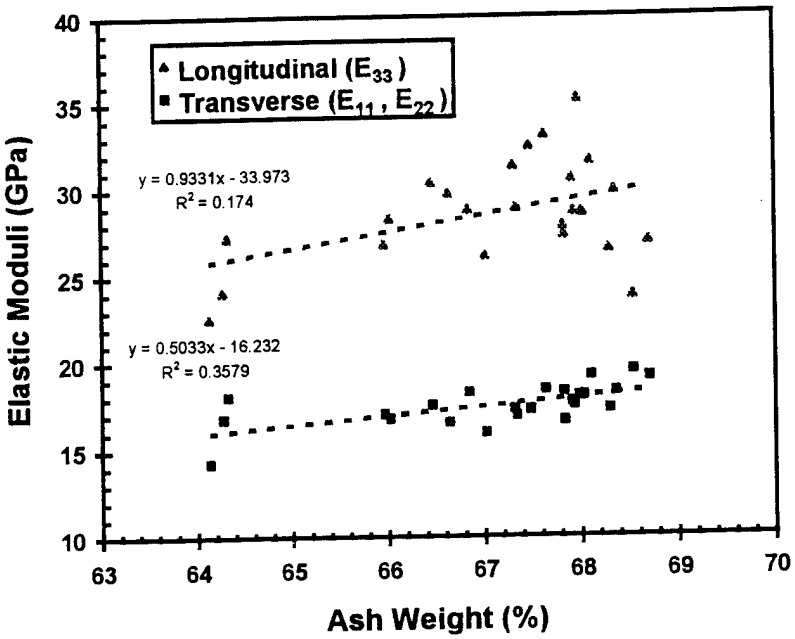

Figure 18. Elastic moduli vs. ash weight.

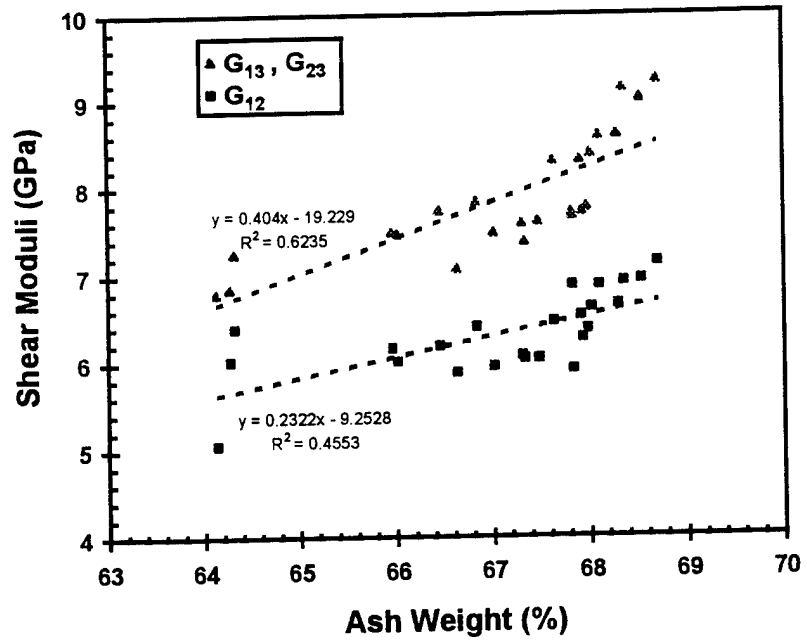

Figure 19. Shear moduli vs. ash weight.

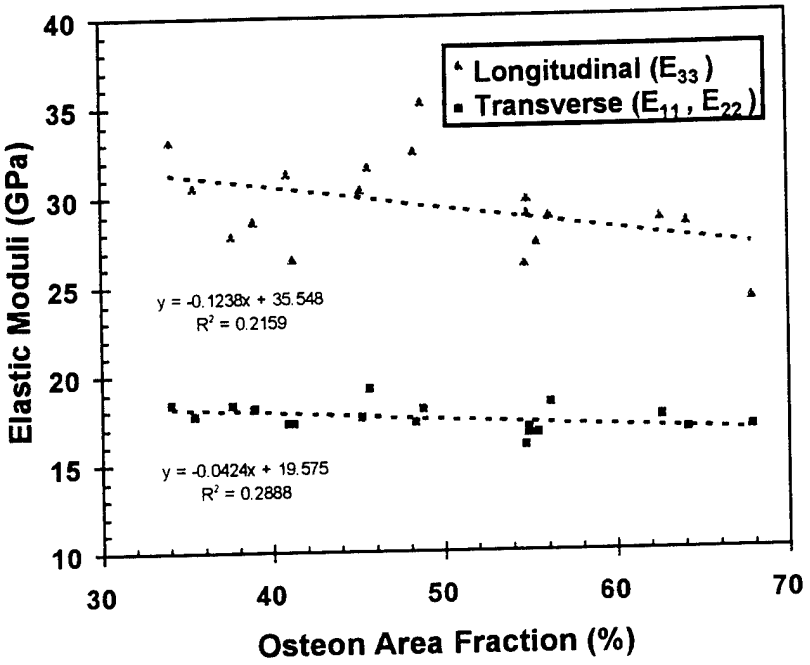

Figure 20. Elastic moduli vs.osteon area fraction.

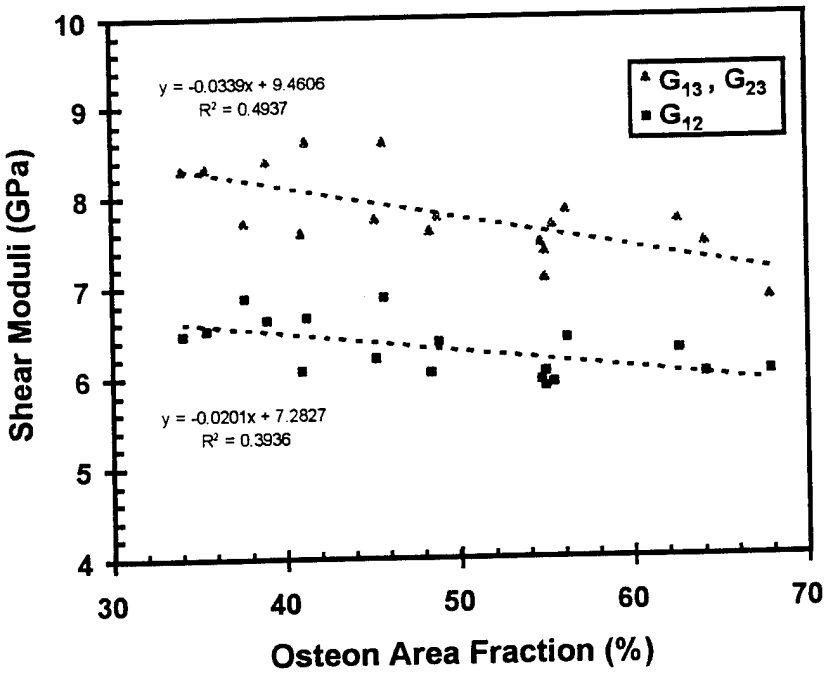

Figure 21. Shear moduli vs. osteon area fraction.

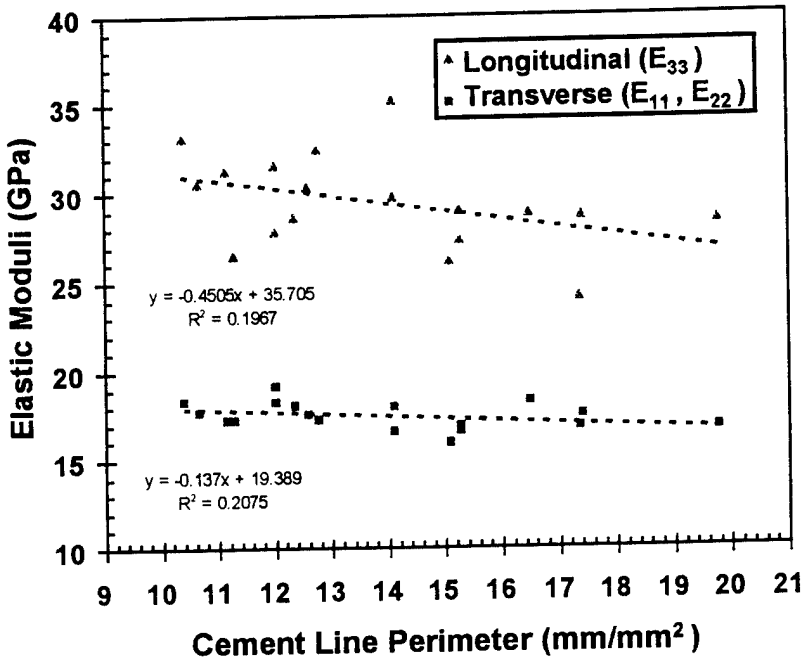

Figure 22. Elastic moduli vs. cement line perimeter.

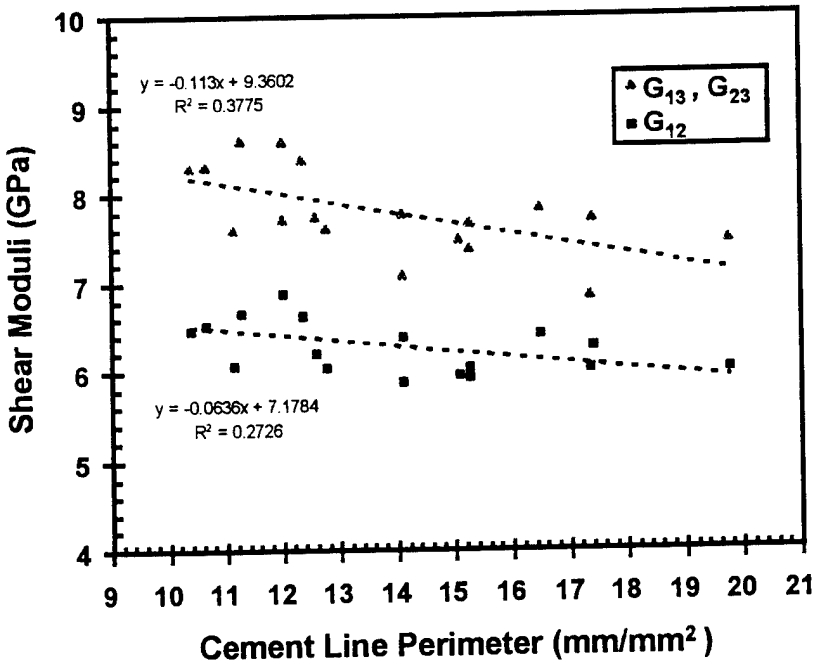

Figure 23. Shear moduli vs. cement line perimeter.

Tensile testing. A total of 12 'dogbone' tensile specimens have been tested thus far in the project. An advantage to tensile testing is the ability to measure strength and related parameters in addition to elastic modulus. The longitudinal elastic moduli and tensile strengths are plotted vs. porosity in Figs. 24 and 25, respectively. Both modulus and strength decrease with porosity but the negative slope for the modulus seems to be steeper than reported above using ultrasonic methods for measuring moduli. Furthermore, the correlation for modulus is rather weak as indicated by the dashed line, but is much better when the results for the two lowest porosity specimens are not included. Additional microstructural analysis is also being conducted for the tensile test specimens. Twelve more specimens have already been machined and are awaiting testing, so the appropriateness of these two data points should become more apparent as more results are obtained. In order to estimate the degree of uniformity, or lack thereof, in the mineralization levels within the tissue microstructure, the mineralization distribution is being determined from the microradiograph images. The Optimas 4.2 image analysis software is again employed in this effort. During the microradiographing procedure, an aluminum step wedge is also exposed with each slice of bone. This provides gray scale levels for defining different degrees of mineralization as 'lowly', 'moderately', or 'highly' mineralized bone tissue. This data, along with cement line perimeter results, should provide considerable insight into the microstructural features and mechanisms responsible for strengthening and stiffening Haversian compact bone tissue. Because these procedures are fairly labor intensive, they are currently still in progress and should be completed in the near future.

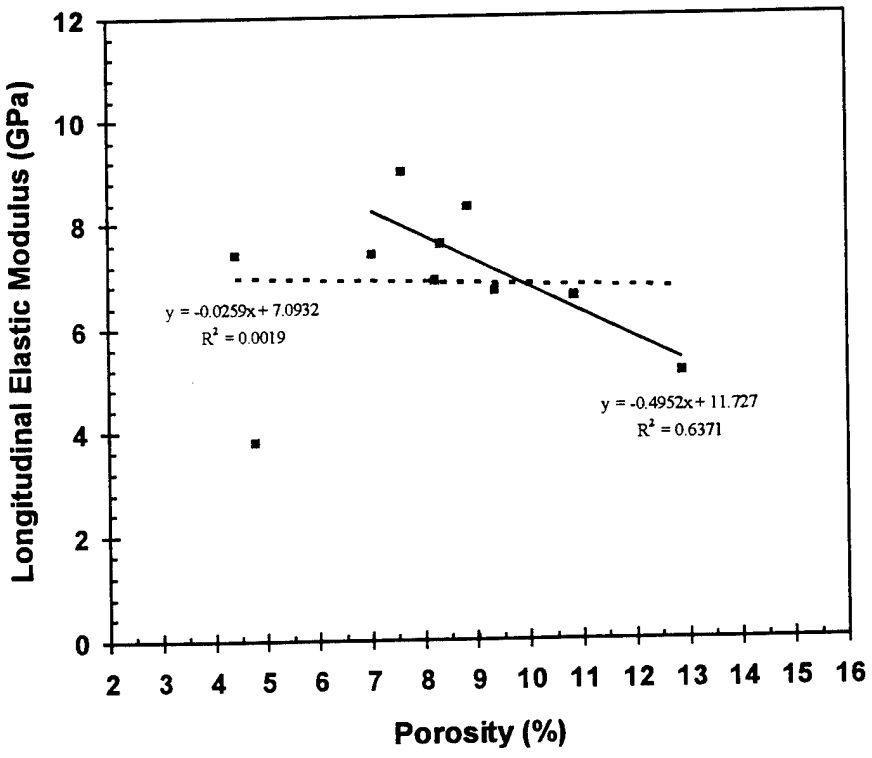

Figure 24. Modulus variation with porosity.

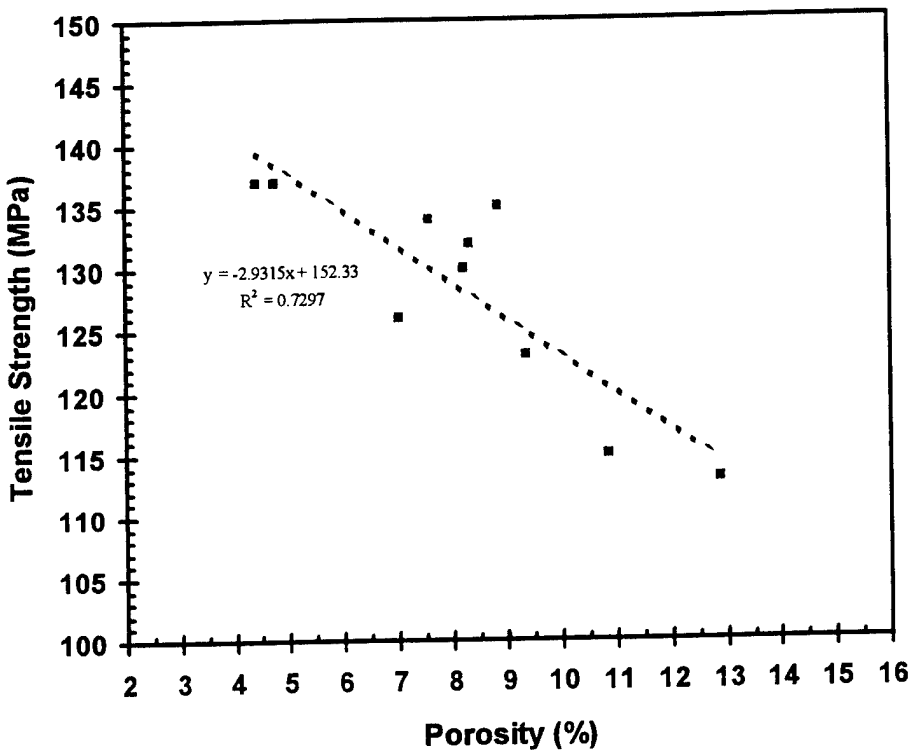

Figure 25. Variation in tensile strength with porosity.

Dynamic mechanical properties. The representative frequency sweep presented previsously in Fig. 12 indicates that the storage (G') and loss (G") moduli only change slightly over the range of frequencies tested. The loss factor (tan δ) decreases over the first two decades and then levels off or increases slightly. Results from the frequency sweep for each specimen were thus summarized in the form of average values for the purposes of correlating with microstructural parameters. The storage and loss moduli are plotted vs. wet and dry density in Figs. 26 and 27, respectively. The storage modulus increases with density, as would be expected, but the loss modulus somewhat surprisingly remains essentially constant over the range of densities tested. Fig. 28 shows a similar trend for moduli vs. % mineralization. Since the purpose of these tests is to seek to detect the influence of the cement line on dynamic properties, the loss factor (which is the ratio of G" to G') is plotted vs. cement line perimeter in Fig. 29. The results reveal a fairly consistent, although mild, decrease in loss factor with increasing cement lines. This is also opposite the expected trend, at least under the hypothesis that the cement line would tend to increase damping within the material. The storage and loss moduli are plotted vs. % secondary Haversian area (SHA) in Figs. 30 and 31. Fig. 30 shows that many samples have very low %SHA, which suggests that they were mainly primary bone and lacked significant Haversian microstructure. Fig. 31 shows the same results but for %SHA greater than 25%. In this case, the storage modulus does in fact decrease with increasing %SHA as has been observed by others (and was also confirmed in our ultrasonic tests reported previously herein). Thus, more conclusive examination of the role of the cement line in damping awaits testing of more samples with predominately Haversian microstructure.

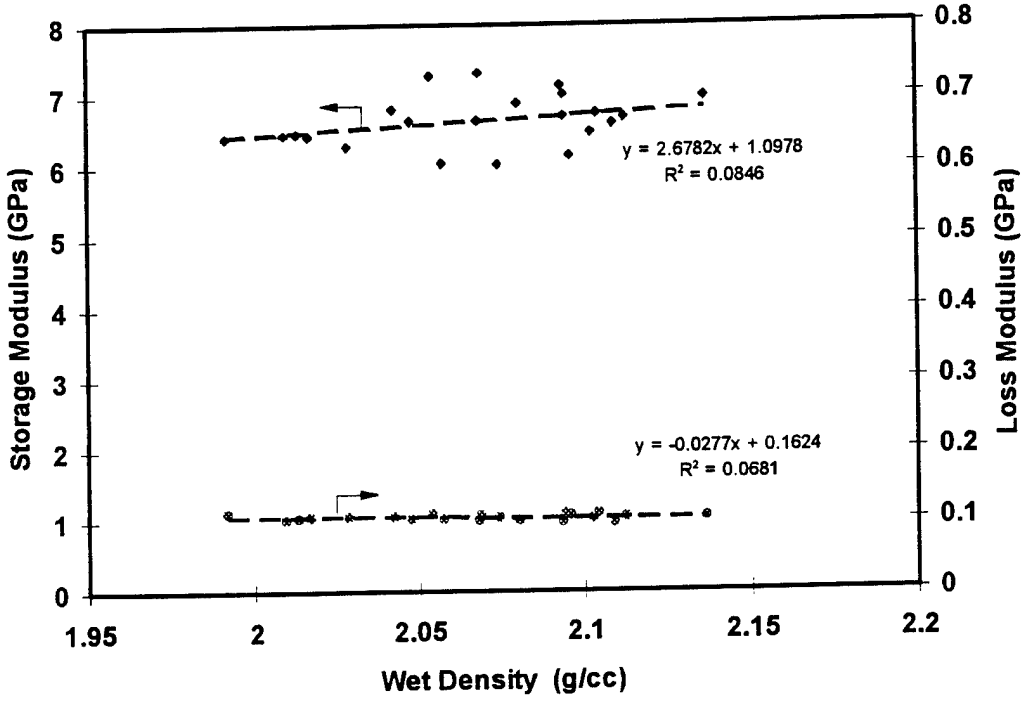

Figure 26. Variation in viscoelastic moduli with wet density.

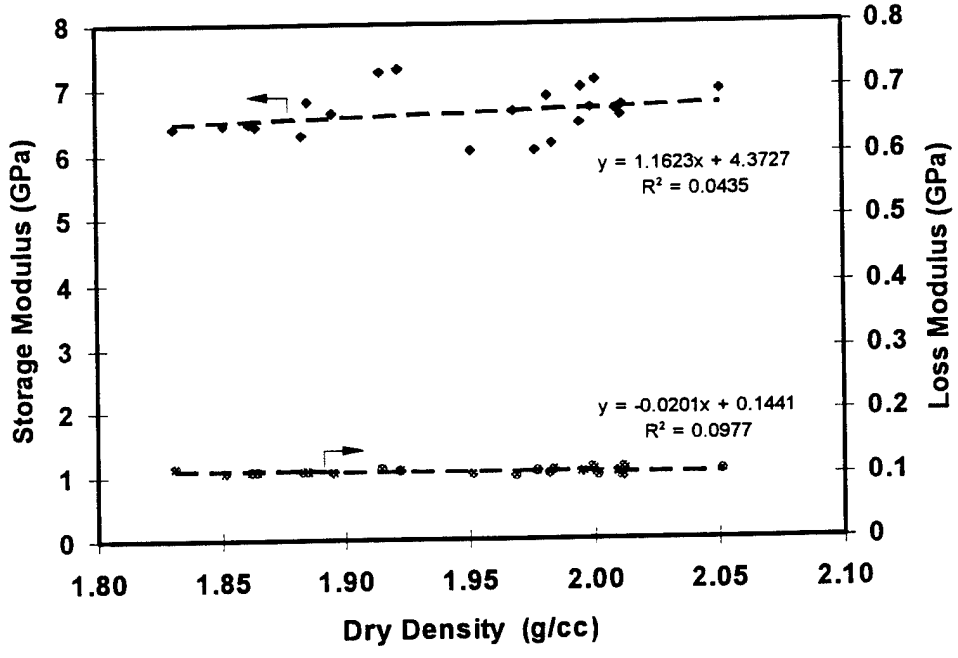

Figure 27. Variation in viscoelastic moduli with dry density.

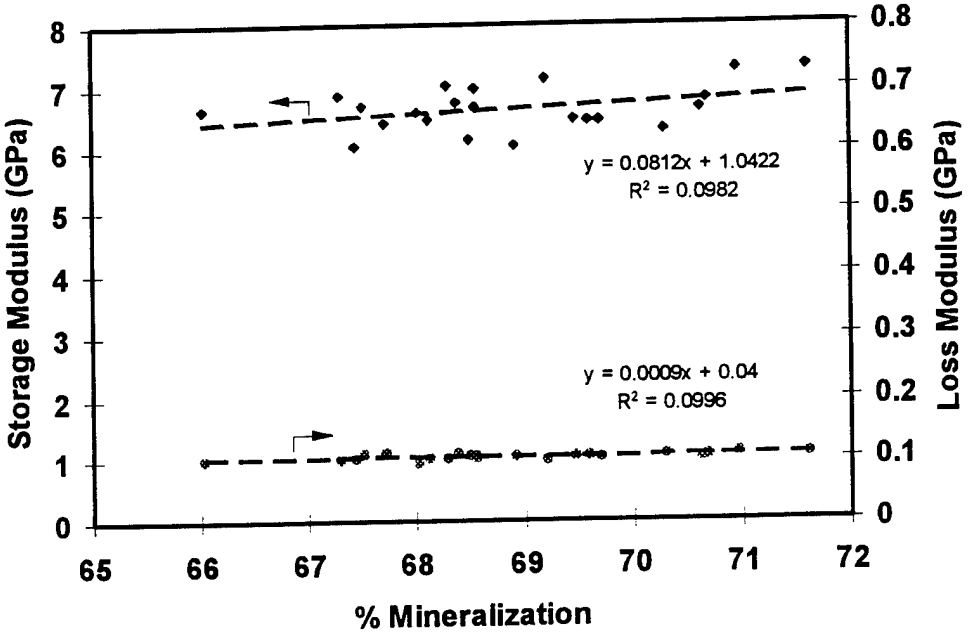

Figure 28. Variation in viscoelastic moduli with ash weight (% mineralization).

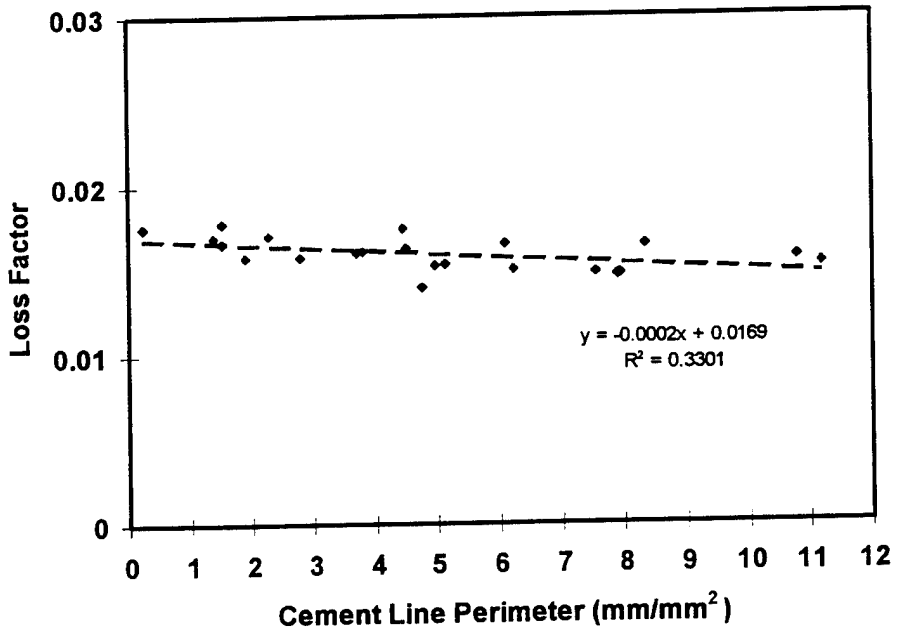

Figure 29. Variation in loss factor with cement line perimeter.

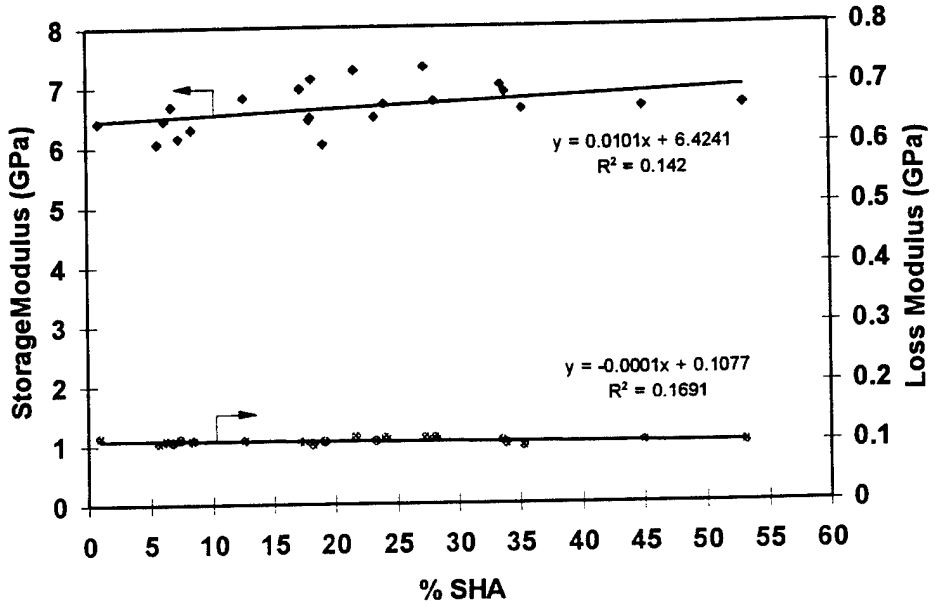

Figure 30. Variation in loss factor with % secondary Haversian area (SHA).

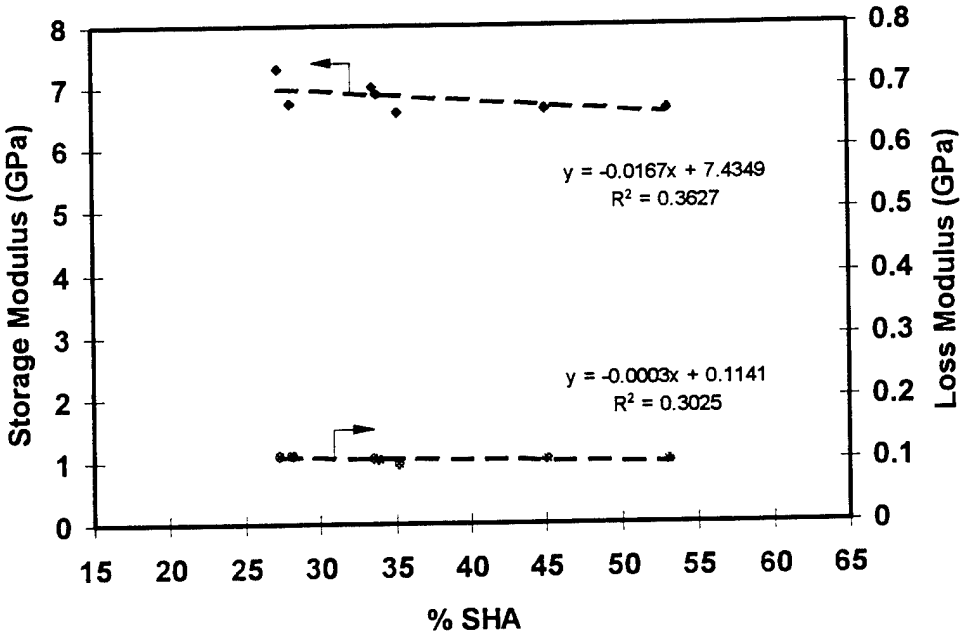

Figure 31. Variation in loss factor with % SHA for predominantly Haversian bone only.

Dissemination of Results

Results from this work have been disseminated regularly in the form of presentations and publications as listed below. Three full-length refereed journal articles are also currently in preparation.

Ayers, A. K., and Hogan, H. A., "Dynamic Mechanical Properties of Equine Compact Bone and Their Dependence Upon Tissue Density," accepted, 1995 Bioengineering Conference, June 28-July 2, 1995, Beaver Creek, CO.

Hogan, H. A., Gunn, K. S., Ahern, J. C., and Simmons, D. J., "Characterizing Osteonal Microstructure and Its Influence Upon the Anisotropic Moduli of Equine Cortical Bone," accepted, 1995 Bioengineering Conference, June 28-July 2, 1995, Beaver Creek, CO.

Ayers, A. K. and Hogan, H. A., "Correlation of Viscoelastic Properties and Microstructure for Equine Cortical Bone Tissue," Abstracts of the Thirteenth Annual Houston Conference on Biomedical Engineering Research, February 16-17, 1995, Houston, TX, p. 97.

Hogan, H. A., Ahern, J. C., and Simmons, D. J., "Variations in the Anisotropic Mechanical Properties of Compact Bone with Tissue Microstructure," Advances in Bioengineering 1994, **BED Vol. 28**, 1994 ASME Winter Annual Meeting, Nov. 6-11, 1994, Chicago, IL, pp. 229-230.

DeFrese, R. J., Ahern, J. C., and Hogan, H. A., "The Anisotropic Mechanical Properties of Compact Bone and Their Correlation with Tissue Microstructure," Recent Advances in Engineering Science, proceedings of the Society of Engineering Science 31st Annual Technical Meeting, October 10-12, 1994, College Station, TX, pp. 255.

Ahern, J. C., Hogan, H. A., and Simmons, D. J., "Relations Between the Ultrasonic Elastic Moduli of Compact Bone and Tissue Microstructure," Biomedical Engineering - Recent Developments, proceedings of the Thirteenth Southern Biomedical Engineering Conference, April 16-17, 1994, Washington, DC, pp. 681-684.

DeFrese, R. J., and Hogan, H. A., "The Effect of Imperfect Cement Line-Osteon Bonding on the Properties of Cortical Bone Tissue," Biomedical Engineering - Recent Developments, proceedings of the Thirteenth Southern Biomedical Engineering Conference, April 16-17, 1994, Washington, DC, pp. 685-688.

Ahern, J. C., and Hogan, H. A., "A Study of Dispersion in the Ultrasonic Velocities of Havesian Compact Bone," Abstracts of the Twelfth Annual Houston Conference on Biomedical Engineering Research, February 10-11, 1994, Houston, TX, p. 93.

DeFrese, R. J., and Hogan, H. A., "Micromechanics Modeling of Compact Bone: Interphase Effects," Abstracts of the Twelfth Annual Houston Conference on Biomedical Engineering Research, February 10-11, 1994, Houston, TX, p. 94.

Hogan, H. A., De Frese, R. J., and Simmons, D. J., "Composite Micromechanics Modeling of Porosity and Interphase Effects in Compact Bone Tissue," presentation to *Seminar in Mechanics and Materials - MEEN 681* class, January 27, 1994.

Hogan, H. A., "Some Biomimetics Problems in Biomechanics," Invited Seminar, joint meeting of A&M Student Chapter of the *Biomedical Engineering Society* and Bioengineering Graduate Seminar Class, Texas A&M University, September 16, 1993, College Station.

Hogan, H. A. and DeFrese, R. J., "Theoretical Modeling of the Effects of Porosity on the Mechanical Properties of Compact Bone Tissue," ISB '93 Resumes/Abstracts, **Vol. I**, International Society of Biomechanics XIVth Congress, July 4-8, 1993, Paris, FRANCE, pp. 582-583.

DeFrese, R. J. and Hogan, H. A., "A Micromechanics Study of the Influence of the Cement Line on the Anisotropy of Compact Bone Tissue," 1993 Bioengineering Conference, **BED Vol. 24**, N. A. Langrana, M. H. Freidman, and E. S. Grood, eds., 1993 ASME/AICHE/ASCE Summer Bioengineering Conference, June 25-29, 1993, Breckenridge, CO, pp. 238-241.

Hogan, H. A. and DeFrese, R. J., "A Comparison of Methods for Including Porosity in Micromechanics Modeling of Compact Bone Tissue," Advances in Experimental Mechanics and Biomimetics, **AD Vol. 29, AMD Vol. 146**, 1992 ASME Winter Annual Meeting, Nov. 8-13, 1992, Anaheim, California, pp. 111-121.

DeFrese, R. J. and Hogan, H. A., "The Influence of Packing Geometry and Fiber/Matrix Interface Conditions on Composite Micromechanics Modeling of Compact Bone Tissue," 1992 ASME Applied Mechanics, Materials and Aerospace Summer Meeting, April 28 -May 1, 1992, Scottsdale, Arizona.

Graduate student research. The research conducted as part of this project has constituted graduate thesis work for the following three graduate students. Please note that the work of John C. Ahern was also partially supported by a grant from the NIH (1 R03 RR06856-01A2).

Raymond J. DeFrese, "Modeling and Characterization of Haversian Cortical Bone as a Fiber Reinforced Composite Material," Ph.D., to graduate December 1995.

Andrew K. Ayers, "Correlations of Mechanical Viscoelastic Properties to Microstructure of Equine Cortical," M.S., August 1995.

John C. Ahern, "Correlations Between the Anisotropic Mechanical Properties of Cortical Bone Tissue and Microstructure," M.S., August 1994.

SUMMARY

The strategy employed in the research conducted under this grant was to first develop a valid theoretical tool for studying the micromechanics of compact bone tissue, and then use this tool to study structure/property relations for potential biomimicking applications. Thus, the early phases of the work focused upon developing and evaluating finite element unit cell micromechanics approaches. Mori-Tanaka effective medium methods were also examined. Due to lack of available results in the literature from other sources, however, focus soon shifted to generating experimental data for verifying and validating the theoretical models. The correlations established from ultrasonic testing suggest that simple 2-D approximations are likely inadequate for micromechanics modeling of Haversian compact bone tissue. In particularly, the dependence of anisotropic moduli upon porosity is opposite the trend expected from a parallel hollow cylinder arrangement of voids (representing the Haversian canal). Thus, future theoretical efforts should be directed at including three-dimensional effects, either directly through 3-D modeling or indirectly through modified or 'quasi' 2-D approaches. These findings are specifically related to predictions of elastic moduli and not necessarily true for strength or dynamic properties. Correlations between tensile strength and microstructure have been initiated during the project period, and are continuing currently in order to include a large enough sample size for meaningful conclusions. More effort than originally expected has been directed during this project toward examining dynamic viscoelastic behavior. Because the cement line present in Haversian compact bone is similar to the compliant interface of brittle composites, dynamic testing has been initiated under the assumption that the cement line will have greater influence upon dynamic behavior than upon static elastic moduli. The results reported herein have established a viable method for such tests. The correlations between loss factor and microstructure are ambiguous because of a large number of specimens that did not possess exclusively Haversian type tissue microstructure. Further work is needed in this area, both experimentally and theoretically. Experimentally, torsion testing will be combined and compared with bending testing as the mode of loading, and a larger number of Haversian bone specimens will be obtained. Both equine and human (and perhaps bovine) bone will be compared as well. In summary, much progress has been made over the project period in defining the important features needed in a valid micromechanics model for compact bone tissue and establishing correlations between macroscopic behavior and quantitative microstructural parameters. With further effort focusing upon dynamic behavior and material strength, more insight should be gained into the unique role of the cement line interphase material and its significance for potential biomimicking applications.

REFERENCES

1. Cowin, S. C., Van Buskirk, W. C., and Ashman, R. B., "Properties of Bone", in *Handbook of Bioengr.* (eds. Skalak, R. & Chien, S.) pp. 2.1-2.27. McGraw-Hill, New York (1987).
2. Bourne, G. H. (ed.), *The Biochemistry and Physiology of Bone, Vol. I: Structure*, 2nd ed., Academic Press, New York (1972).
3. Swanson, S. A. W., "Biomechanical Characteristics of Bone", *Advances in Biomedical Engineering*, vol. 1 (edited by Kenedi, R. M.). Academic Press, New York (1971).
4. Martin, R. B., "Porosity and Specific Surface of Bone", *CRC Critical Reviews in Biomedical Engineering*, **10**, pp. 179-222 (1984).
5. Hogan, H. A., "Micromechanics Modeling of Haversian Cortical Bone Properties", *J. Biomechanics*, Vol. 25, No. 5, pp. 549-556 (1992).
6. Zhao, Y. H., Tandon, G. P. and Weng, G. J., "Elastic Moduli for a Class of Porous Materials", *Acta Mechanica*, **76**, pp. 105-130 (1989).
7. Schaffler, M. B. and Burr, D. B., "Stiffness of Compact Bone: Effects of Porosity and Density", *J. Biomechanics*, Vol. 21, No. 1, pp. 13-16 (1988).
8. Bert, C.W., "Prediction of Elastic Moduli of Solids With Oriented Porosity," *J. Mat. Sci.* **20**, 2220-2224 (1985).
9. Cowin, S.C. (ed.), *Bone Mechanics*, CRC Press, Boca Raton, FL. (1989).
10. Burr, D. B., Schaffler, M. B., and Frederickson, R. G., "Composition of the Cement Line and its Possible mechanical Role as a Local Interface in Human Compact Bone," *J. Biomechanics*, **21**, pp. 939-945 (1988).
11. Lakes, R and Saha, S., "Cement Line Motion in Bone," *Science* **204,** 501-503 (1979).
12. Martin, R.B. and Burr, D.B., *Structure, Function and Adaptation of Compact Bone,* Raven Press, New York (1989).
13. Dasgupta, A. and Bhandarkar, S. M., "A Generalized Self-consistent Mori-Tanaka Scheme for Fiber Composites with Multiple Interphases", *Mech. Mater.* **14,** pp. 67-82 (1992).
14. Katz, J. L., "Composite Material Models for Cortical Bone", *Mechanical Properties of Bone* (Edited by Cowin, S. C.) AMD Vol. 45, pp. 171-184, American Society of Mechanical Engineers, New York (1981).
15. Pidaparti, R. M. V. and Burr, D. B., "Collagen Fiber Orientation and Geometry Effects on the Mechanical Properties of Secondazry Osteons," *J. Biomechanics*, **25**, pp. 869-880 (1992).
16. Ashman, R. B., "Ultrasonic Determination of the Elastic Properties of Cortical Bone: Techniques and Limitations," Ph.D. Dissertation, Tulane University, (1982).
17. McCalden, R. W., McGeough, J. A., Barker, M. B., and Court-Brown, C. M., "Age-Related Changes in the Tensile Properties of Cortical Bone," *J. Bone Jt. Surg.*, **75-A**, pp. 1193-1205 (1993).
18. Evans, F. G., "Relations Between the Microscopic Structure and Tensile Strength of Human Bone", *Acta. Anat.* **35**, pp. 285-301 (1958).
19. Vincentelli, R. and Grigorov, M., "The Effect of Haversian Remodeling on the Tensile Properties of Human Cortical Bone," *J. Biomech.*, Vol. 18, No. 3, pp. 201-207 (1985).
20. Saha, S. and Hayes, W. C., "Relations Between Tensile Impact Properties and Microstructure of Compact Bone", *Calc. Tiss. Res.*, Vol. 24, pp. 65-72 (1977).